TABLE 1

Dual up-regulated genes by 48-h treatment with vitamin K_2 (10 μM) or RIF (10 μM) in MG63/FLAG-VP16C-SXR cells identified by GeneChip analysis

Gene annotation was determined based on the probe set ID by the Array Finder on the Affymetrix web site.

Probe set ID	Ensemble ID	Gene symbol	Description	-Fold increase over control	
				Vitamin K_2	RIF
209994_s_at	ENSG00000085563	*ABCB1*	ATP-binding cassette, subfamily B (MDR/TAP), member 1	6.06	4.29
209993_at	ENSG00000085563	*ABCB1*	ATP-binding cassette, subfamily B (MDR/TAP), member 1	4.29	4.00
205357_s_at	ENSG00000144891	*AGTR1*	Angiotensin II receptor, type 1	2.83	2.46
212938_at	ENSG00000142156	*COL6A1*	Collagen, type VI, α1	2.64	2.14
201743_at	ENSG00000170458	*CD14*	CD14 antigen	2.46	4.92
209771_x_at	ENSG00000185275	*CD24*	CD24 antigen (small cell lung carcinoma cluster 4 antigen)	2.46	2.30
211839_s_at	ENSG00000184371	*CSF1*	Colony-stimulating factor 1 (macrophage)	2.46	2.30
212937_s_at	ENSG00000142156	*COL6A1*	Collagen, type VI, α1	2.46	2.14
216379_x_at	ENSG00000185275	*CD24*	CD24 antigen (small cell lung carcinoma cluster 4 antigen)	2.46	2.30
202350_s_at	ENSG00000132561	*MATN2*	Matrilin-2	2.30	6.96
203632_s_at	ENSG00000167191	*GPRC5B*	G protein-coupled receptor, family C, group 5, member B	2.30	5.28
211653_x_at	ENSG00000151632	*AKR1C2*	Aldo-keto reductase family 1, member C2	2.30	3.73
218245_at	ENSG00000182704	*TSK*	Likely ortholog of chicken tsukushi	2.30	2.64
218854_at	ENSG00000111817	*SART2*	Squamous cell carcinoma antigen recognized by T cells 2	2.30	5.28
210002_at	ENSG00000141448	*GATA6*	GATA-binding protein 6	2.14	2.14
216594_x_at	ENSG00000187134	*AKR1C1*	Aldo-keto reductase family 1, member C1	2.14	3.73
204151_x_at	ENSG00000187134	*AKR1C1*	Aldo-keto reductase family 1, member C1	2.00	3.48
212268_at	ENSG00000021355	*SERPINB1*	Serine (or cysteine) proteinase inhibitor, clade B (ovalbumin), member 1	2.00	2.83

(*TSK*), an extracellular matrix protein matrilin-2 (*MATN2*), and CD14 antigen.

Ligand-dependent Induction of SXR Target Genes in Osteoblastic Cells—We next validated whether mRNA expression levels for these three genes could be modulated by vitamin K_2 and RIF in MG63 cells ectopically expressing either FLAG-VP16C-SXR or FLAG-SXR using quantitative real-time RT-PCR analysis (Fig. 2). All of the three SXR target genes, *TSK*, *MATN2*, and *CD14*, were up-regulated by SXR ligands. The time-dependent expression profiles of those genes in FLAG-VP16C-SXR and FLAG-SXR-expressing cells were quite similar, although the amplitude of induction was different in these cells. In both cell types, RIF generated stronger induction of mRNA expression than vitamin K_2. Nevertheless, the maximal induction by vitamin K_2 was greater than 2-fold for all three genes in both cell types.

Transcriptional Regulation of SXR Target Genes in Osteoblastic Cells—We next asked whether the induction of SXR target genes was dependent on direct activation of transcription or required ongoing protein synthesis. MG63 cells overexpressing FLAG-SXR were treated with vitamin K_2 or RIF in the presence or absence of cycloheximide. The ligand-dependent up-regulation of the three SXR target genes, including *TSK*, *MATN2*, and *CD14*, was not affected by cycloheximide treatment, indicating that the transcriptional regulation of those genes was independent of protein synthesis (Fig. 3*A*).

To further demonstrate the requirement for SXR in the regulation of *TSK*, *MATN2*, and *CD14*, we investigated the effects of siRNA on the ligand-dependent induction of gene expression. Forty-eight hour treatment with a specific siRNA duplex against SXR (siRNA-SXR), but not with a control siRNA directed against luciferase (siRNA-Luc), reduced the SXR protein level by more than 60% in MG63/SXR clone #3 (Fig. 3*B*). The effectiveness of the SXR-specific siRNA was confirmed as the vitamin K_2-induced up-regulation of CYP3A4 mRNA expression was diminished by the SXR siRNA in MG63/SXR clone #3 (Fig. 3*C*). In that cell system, the SXR siRNA significantly reduced either vitamin K_2- or RIF-activated mRNA expression for *TSK*, *MATN2*, and *CD14* (Fig. 3*D*).

We next examined whether the SXR siRNA duplex reduced the endogenous expression of SXR protein (Fig. 4). The endogenous level of SXR protein in parental MG63 cells was barely detected in Western blot analysis (Fig. 4*A*). Thus, we immunoprecipitated MG63 cell lysates with a polyclonal antibody against the hinge and a part of ligand-binding domain of SXR (H-160) and immunodetected SXR protein by another polyclonal antibody against the SXR N terminus (N-16). The enrichment of SXR protein in immunoprecipitated fraction was also confirmed in COS1 cells transiently transfected with FLAG-SXR (Fig. 4*A*). Based on this evaluation system, we could show that the SXR siRNA reduced the level of endogenous SXR protein in MG63 (Fig. 4*B*).

Since we confirmed that the SXR siRNA duplex was effective to inhibit the endogenous expression of SXR protein, we next analyzed whether the SXR siRNA reduced the expression of the SXR target genes in parental MG63 cells. The SXR siRNA at 14 or 70 nM could significantly reduce endogenous SXR mRNA levels in natural MG63 cells (Fig. 4*C*). The expression of *TSK*, *MATN2*, and *CD14* was all up-regulated by either vitamin K_2 or RIF, indicating that the three genes were *bona fide* SXR targets in parental MG63 cells (Fig. 4*D*). This ligand-dependent induction of all three genes was significantly reduced by the SXR siRNA transfection in parental MG63 cells (Fig. 4*D*).

Vitamin K_2 and TSK Stimulate Collagen Accumulation in Osteoblastic Cells—TSK was recently identified as a bone morphogenic protein-binding protein that belongs to the small leucin-rich proteoglycan family (21), which is implicated as an extracellular matrix component. Because small leucine-rich proteoglycans such as biglycan and decorin are known to interact with matrilin-1 in the cartilage extracellular matrix (22), TSK and matrilin-1-related MATN2 are likely to be involved in the assembly of extracellular matrix, including collagens, in osteoblastic cells.

We next asked whether vitamin K_2 promoted collagen production or stabilized collagen levels. We evaluated collagen amounts by staining cells with a strong anionic dye Sirius red, which reacted with basic groups present in collagens via its sulfonic acid groups. It has been reported that type I and III collagens are well stained by Sirius red (19). Four-day treatment with vitamin K_2 exhibited significantly more intense staining by Sirius red compared with vehicle in MG63 cells under conditions favoring osteoblast differentiation (Fig. 5*A*). We also examined collagen accumulation in murine MC3T3-E1 cells, one of the cell lines with a close-to-normal osteoblast phenotype. Four-day treatment with vitamin K_2 increased collagen accumulation by 15.0% in this cell line. Note that RIF (1 μM) also increased collagen accumulation by 13.6% in MG63 cells after 4-day treatment. Moreover, the vitamin K_2-stimulated collagen accumulation in MG63 cells was not affected by warfarin treatment, suggesting that the γ-carboxylase-dependent vitamin K_2 action may not be involved (Fig. 5*B*).

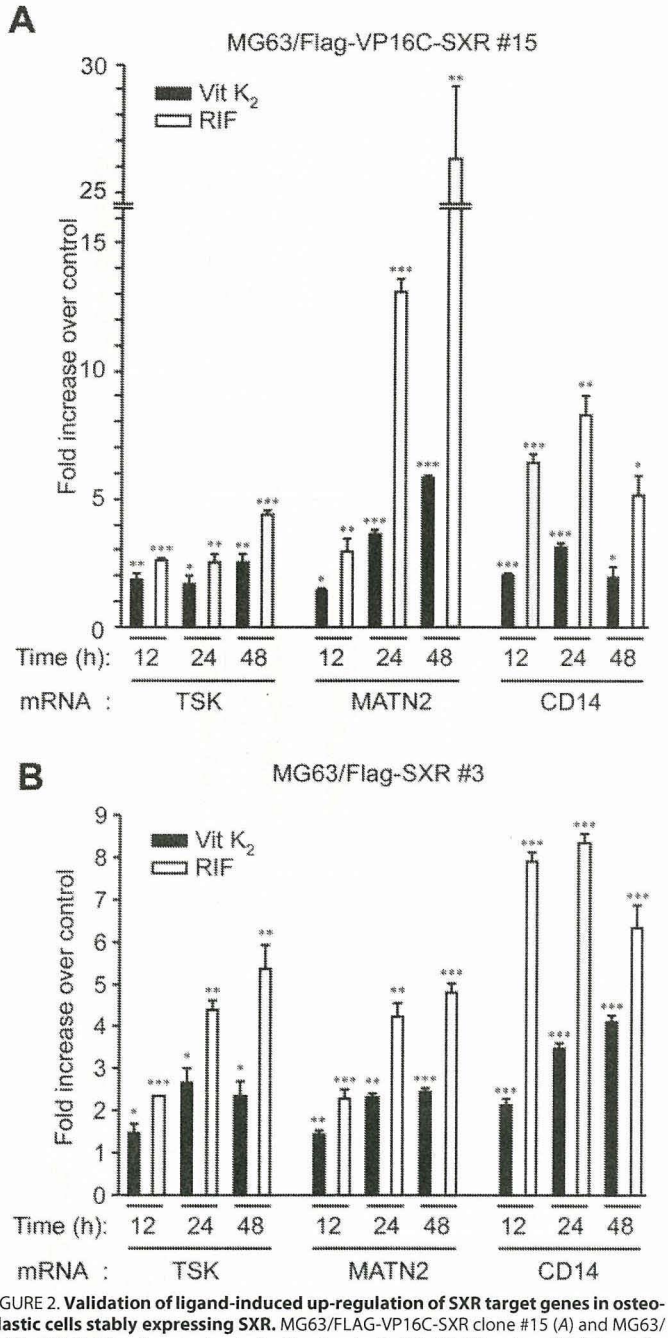

FIGURE 2. **Validation of ligand-induced up-regulation of SXR target genes in osteoblastic cells stably expressing SXR.** MG63/FLAG-VP16C-SXR clone #15 (*A*) and MG63/FLAG-SXR #3 (*B*) cells were treated with vitamin K_2 (*Vit K_2*) (10 μM) or RIF (10 μM) for indicated times. mRNA levels for tsukushi (*TSK*), *MATN2*, and *CD14* were determined by quantitative RT-PCR using *GAPDH* as an external control. Data represent fold induction of mRNA levels by ligands *versus* vehicle. *, $p < 0.05$; **, $p < 0.01$; ***, $p < 0.001$ (by Student's *t* test).

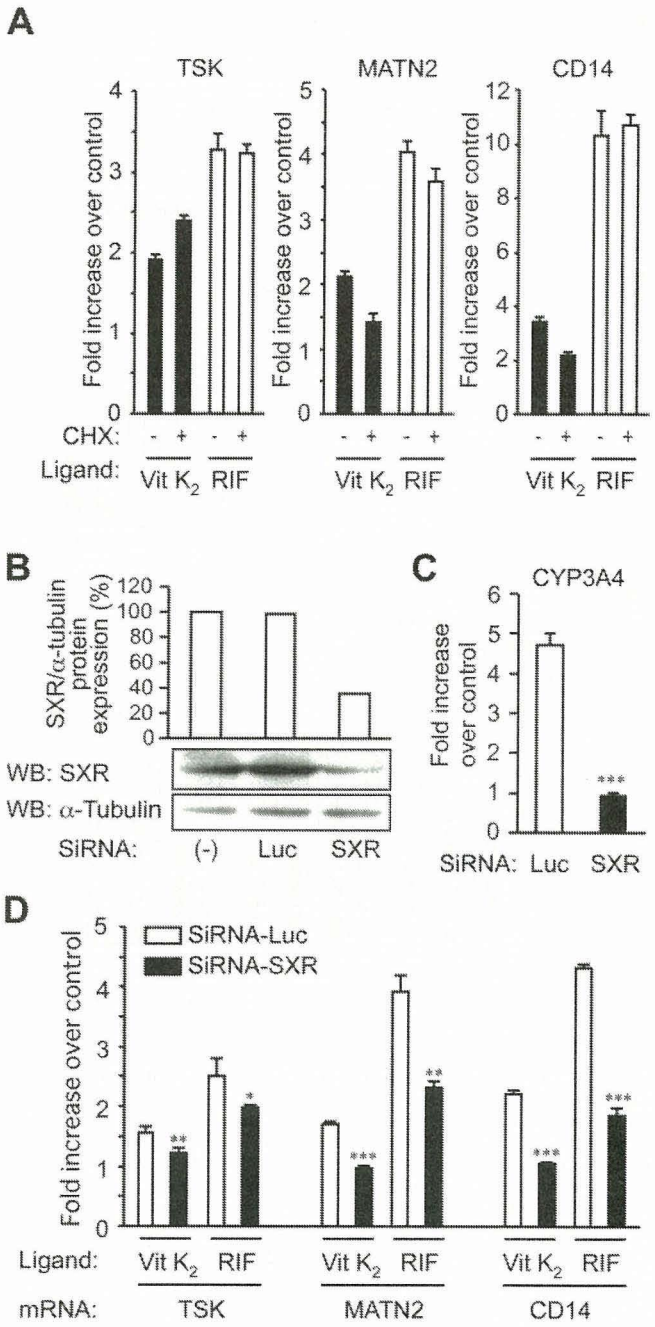

FIGURE 3. **Ligand-induced up-regulation of TSK, MATN2, and CD14 are directly regulated by SXR.** *A*, effects of cyclohexamide (*CHX*) on transcription of SXR target genes. MG63/FLAG-SXR #3 cells were pretreated with CHX (10 μg/ml) or vehicle for 2 h, then stimulated by vitamin K_2 (*Vit K_2*) (10 μM) or RIF (10 μM) for 24 h. *B*, reduction of SXR expression by siRNA directed against SXR. MG63/FLAG-SXR cells #3 were transfected with siRNA against luciferase (*Luc*) or SXR (70 nM each) for 48 h. The SXR protein level was analyzed by Western blotting (*WB*). Data in the *upper graph* represent quantified levels of SXR normalized to α-tubulin as determined by NIH image software. *C*, effects of SXR siRNA transfection on vitamin K_2-induced up-regulation of *CYP3A4* mRNA in MG63/FLAG-SXR #3 cells. *D*, effects of SXR siRNA transfection on ligand-induced up-regulation of *TSK*, *MATN2*, and *CD14* mRNA in MG63/FLAG-SXR #3 cells. *, $p < 0.05$; **, $p < 0.01$; ***, $p < 0.001$ (by Student's *t* test).

To determine whether TSK plays a role in the vitamin K_2-stimulated collagen accumulation, MG63 cells stably expressing FLAG-tagged TSK were generated. Two TSK-overexpressing clones were isolated, as confirmed by Western blot analysis (Fig. 5*C*). MG63 clones overexpressing TSK showed significantly enhanced collagen accumulation in 7-day culture under differentiation conditions compared with vector-transfected cells (Fig. 5*D*). During the 7-day culture, the growth of MG63 clones expressing TSK and vector was almost stationary, and there was no significant difference in proliferation between the two groups as determined by the proliferation assay using WST-8 (2-(2-methoxy-4-nitrophenyl)-3-(4-nitrophenyl)-5-(2,4-disulfophenyl)-2*H*-tetrazolium monosodium salt) reagent (Nacalai Tesque, Kyoto, Japan; Ref. 23) (data not shown).

We further investigated whether SXR or TSK loss-of-function affected collagen accumulation in MG63 cells. A siRNA duplex against *TSK* (70 nM) reduced the target mRNA levels by more than 40% in parental MG63 cells, verifying its efficiency (Fig. 6*A*). The *SXR*- and *TSK*-specific siRNA significantly reduced the vitamin K_2-stimulated

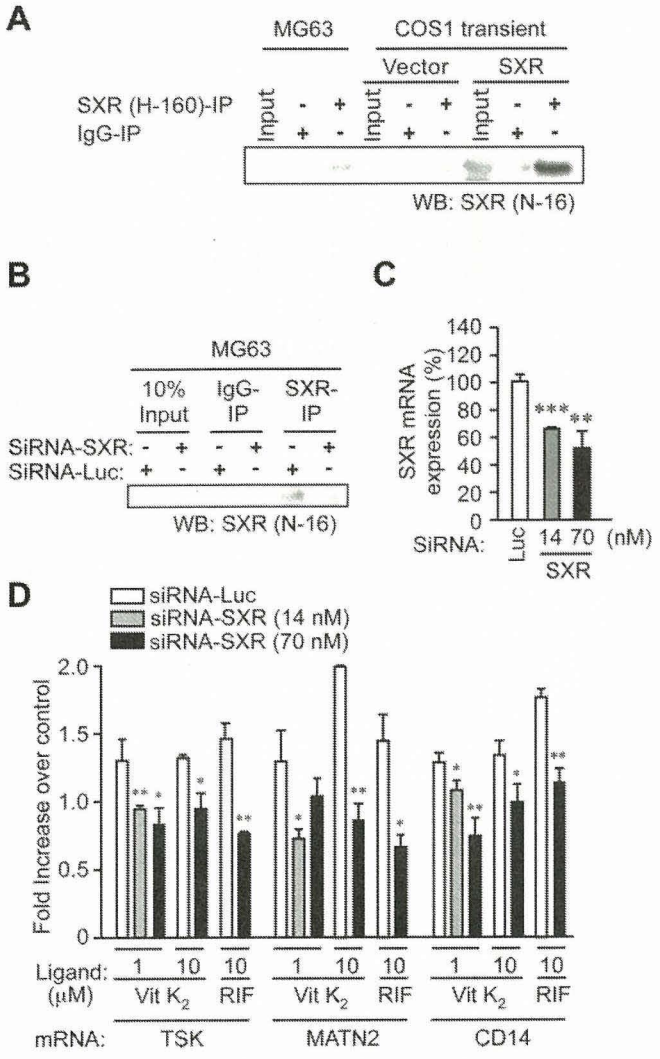

FIGURE 4. ***SXR* siRNA represses ligand-induced up-regulation of SXR target genes in osteoblastic cells.** *A*, detection of endogenous SXR protein enriched by immunoprecipitation (*IP*) in parental MG63 cells. Lysates from MG63 cells and COS1 cells transiently transfected with SXR or empty vector were immunoprecipitated by anti-SXR antibody (H-160), and SXR protein was immunodetected by anti-SXR (N-16) antibody. *B*, reduction of SXR protein level by *SXR* siRNA in MG63 cells. Cells were transfected with *SXR* or luciferase (*Luc*) siRNA for 48 h, and SXR protein level was analyzed as described for *A*. *C*, concentration-dependent effects of *SXR* siRNA on endogenous *SXR* mRNA levels in MG63 cells. Cells were transfected with *SXR* siRNA or control luciferase siRNA at the indicated concentrations for 24 h. *D*, effects of *SXR* siRNA on ligand-induced up-regulation of *TSK*, *MATN2*, and *CD14* mRNA in MG63 cells. After 48-h treatment with siRNA (14 or 70 nM), cells were stimulated with vitamin K_2 (1 or 10 μM) or RIF (10 μM) for 12 h. *, $p < 0.05$; **, $p < 0.01$; ***, $p < 0.001$ (by Student's *t* test). *WB*, Western blotting.

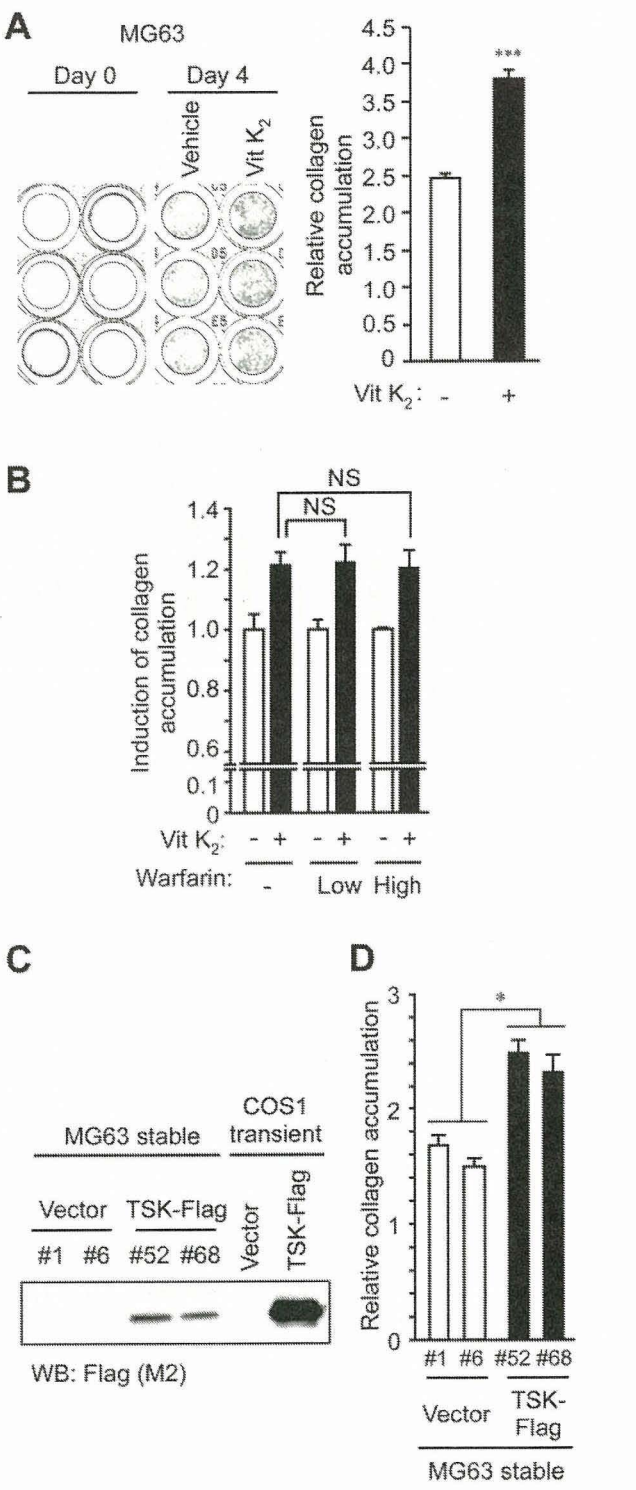

FIGURE 5. **Vitamin K_2 (*Vit K_2*) and TSK expression promote collagen accumulation in osteoblastic cells.** *A*, MG63 cells at confluence were maintained in osteoblast differentiation medium containing ascorbic acid and β-glycerophosphate in the presence or absence of vitamin K_2 (1 μM) for 4 days, and collagen accumulation was analyzed by Sirius red staining (*left panel*). The collagen level was quantified by the absorbance at 550 nm (*right panel*). ***, $p < 0.001$ (by Student's *t* test). *B*, the vitamin K_2-stimulated collagen accumulation was not affected by a γ-carboxylase inhibitor warfarin. Cells at confluence were pretreated with vehicle or warfarin (low, 5 μM; high, 25 μM) for 1 day and incubated with vehicle or vitamin K_2 (1 μM) for another 3 days (warfarin final concentration; low, 2.5 μM; high, 12.5 μM). *NS*, not significant. *C*, generation of MG63 cells stably expressing TSK-FLAG construct. Expression of TSK protein in MG63/TSK-FLAG clones #52 and #68 was immunodetected by anti-FLAG antibody. *D*, TSK overexpression augments collagen accumulation in MG63 cells. Cells at confluence were maintained in the differentiation medium for 7 days, and collagen accumulation was analyzed by Sirius red staining as described for *A*. *, $p < 0.05$ (by Student's *t* test). *WB*, Western blotting.

accumulation of collagen in parental MG63 cells compared with luciferase siRNA (Fig. 6, *B* and *C*).

Taken together, our results indicate that vitamin K_2 promotes collagen accumulation in osteoblastic cells via the SXR signaling pathway.

DISCUSSION

In the present study, we identified novel SXR target genes that are up-regulated by both vitamin K_2 and RIF in osteoblastic cells using oligonucleotide microarrays. The effectiveness of vitamin K_2 and RIF treatment was evident by their ability to up-regulate mRNA levels for the well known SXR target gene MDR1. SXR-dependent induction of TSK, MATN2, and CD14 has not been previously reported. Functional analyses indicated that vitamin K_2 can enhance collagen accumulation in osteoblastic cells and that SXR may play a role in the collagen assembly mechanism. Taken together, these results provide important evi-

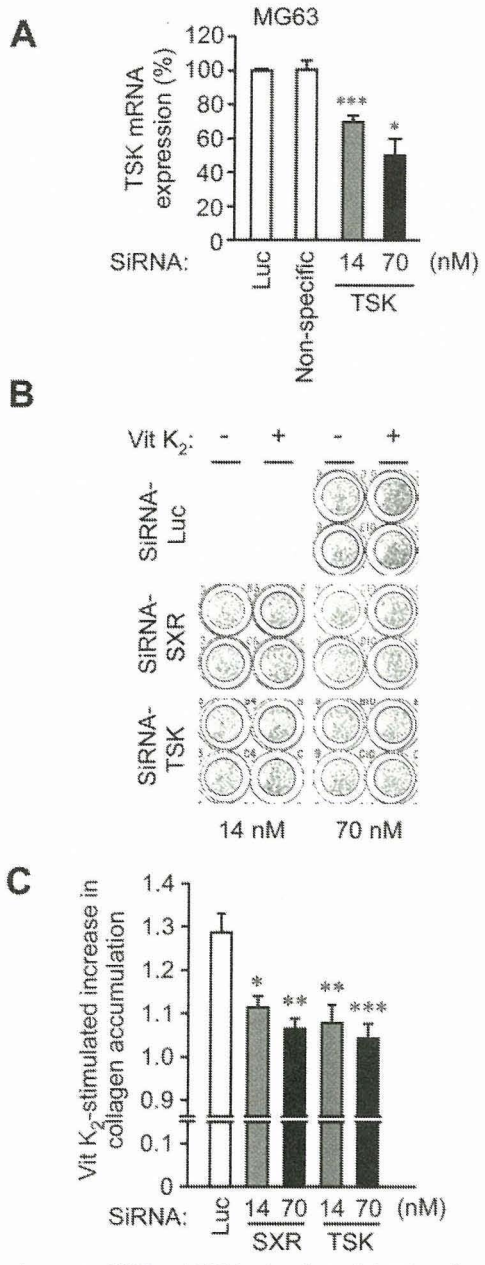

FIGURE 6. **Involvement of SXR and TSK in vitamin K_2 (*Vit K_2*)-mediated collagen accumulation.** *A*, effects of *TSK*-specific siRNA on *TSK* mRNA level in MG63 cells. Cells were transfected with luciferase (*Luc*) siRNA, nonspecific siRNA, or *TSK* siRNA (14 or 70 nM) for 48 h. *B*, *SXR* and *TSK* siRNAs reduce vitamin K_2-mediated collagen accumulation in MG63 cells. Confluent cells in differentiation medium were transfected with siRNA at the indicated concentrations twice every 2 days. Collagen accumulation in 4-day culture in the presence of vitamin K_2 (1 μM) or vehicle was determined by Sirius red staining. *C*, vitamin K_2-stimulated increase in collagen accumulation in *B* was quantified by the absorbance at 550 nm. Each column shows fold induction by vitamin K_2 normalized to that by vehicle and indicated siRNA treatment. *, $p < 0.05$; **, $p < 0.01$; ***, $p < 0.001$ (by Student's *t* test, using the fold induction by vitamin K_2 in Luc siRNA-treated cells as a control).

dence that vitamin K_2 directly activates SXR to promote extracellular matrix formation in osteoblastic cells.

While vitamin K has been well characterized as a cofactor of γ-carboxylase, we have previously showed that vitamin K_2 could have an anabolic effect on osteoblasts by up-regulating the mRNA levels for bone marker genes through SXR (13). Our present findings that vitamin K_2 promotes extracellular matrix formation by activating SXR to up-regulate the *TSK* mRNA level provides further evidence that vitamin K_2 stimulates bone formation via altering gene expression.

The vitamin K_2-stimulated collagen accumulation through the activation of SXR signaling may be beneficial to decrease bone fractures. Since bone collagen content is reduced in aged and osteoporotic bones (24), the amount and quality of collagen fibrils may be important for maintaining bone strength. Therefore, in addition to its role as an enzymatic cofactor that facilitates γ-carboxylation of bone Gla proteins, vitamin K_2 may serve as a critical factor regulating bone matrix formation.

The identification of new SXR-mediated vitamin K_2 target genes in bone cells has implications for bone homeostasis. Human TSK is an ortholog of chicken TSK, which was recently identified as a bone morphogenic protein-binding protein that plays a role in the development of primitive streak and Hensen's node formation during chick gastrulation (21). TSK, like other small leucine-rich proteoglycans, may play a role in bone formation. Small leucine-rich proteoglycans such as biglycan, decorin, and chondroadherin have been characterized as collagen-binding proteins in bone tissues (25–28). Biglycan-deficient mice exhibit reduced bone mass (29), and biglycan/decorin double-deficient mice show a more severe phenotype of osteoporosis (30).

MATN2 is expressed in various osteoblastic cells as well as mouse primary osteoblasts (31, 32), and it was shown to interact with collagen I (33). The involvement of matrilin proteins together with small leucine-rich proteoglycans in the collagen assembly is exemplified by the complex of matrilin-1 and biglycan/decorin that act as a linkage between the collagen II and collagen VI fibrils (22).

The CD14 antigen is a lipopolysaccharide-binding protein expressed in monocytes where it initiates the innate immune response to bacterial invasion (34). The soluble form of CD14 is an inducer of B-lymphocyte growth and differentiation (35), and B-lymphocyte lineage cells regulate osteoclastogenesis by expressing receptor activator of NF-κB ligand (RANKL) and serving as osteoclast progenitor cells (36). This suggests a role for CD14 in osteoclastogenesis through B-lymphocyte lineage cells. A role for CD14 in bone formation is also suggested by a report showing that the antigen was up-regulated during the differentiation of mouse primary osteoblasts (37). Because osteoclastic resorption and osteoblast formation are coupled in the bone remodeling process, CD14 may play a role as a "coupling factor" between the two functions. In this context, it is interesting that CD24 was identified as an up-regulated gene by both vitamin K_2 and RIF in osteoblastic cells in our microarray analysis because CD24 is also a cell surface antigen predominantly expressed in B-cell lineage cells and it has been implicated in both activation and differentiation of B lymphocytes (38).

In summary, we conclude that SXR mediates vitamin K_2-activated transcription of extracellular matrix-related genes as well as cell surface markers of B-lymphoid lineage cells that may be involved in both osteoblastogenesis and osteoclastogenesis. These results would provide new insight into vitamin K_2 and SXR action on bone homeostasis and osteoporosis treatment and further support the idea that vitamin K_2 acts as a transcriptional mediator of gene expression in bone cells, in addition to its well known role as an enzymatic cofactor.

Acknowledgments—We thank T. Suzuki and R. Nozawa for their technical assistance.

REFERENCES

1. Akedo, Y., Hosoi, T., Inoue, S., Ikegami, A., Mizuno, Y., Kaneki, M., Nakamura, T., Ouchi, Y., and Orimo, H. (1992) *Biochem. Biophys. Res. Commun.* **187,** 814–820
2. Akiyama, Y., Hara, K., Tajima, T., Murota, S., and Morita, I. (1994) *Eur. J. Pharmacol.* **263,** 181–185
3. Hara, K., Akiyama, Y., Nakamura, T., Murota, S., and Morita, I. (1995) *Bone (N.Y.)* **16,** 179–184

4. Koshihara, Y., and Hoshi, K. (1997) *J. Bone Miner. Res.* **12,** 431–438
5. Koshihara, Y., Hoshi, K., Okawara, R., Ishibashi, H., and Yamamoto, S. (2003) *J. Endocrinol.* **176,** 339–348
6. Shiraki, M., Shiraki, Y., Aoki, C., and Miura, M. (2000) *J. Bone Miner. Res.* **15,** 515–521
7. Booth, S. L., Tucker, K. L., Chen, H., Hannan, M. T., Gagnon, D. R., Cupples, L. A., Wilson, P. W., Ordovas, J., Schaefer, E. J., Dawson-Hughes, B., and Kiel, D. P. (2000) *Am. J. Clin. Nutr.* **71,** 1201–1208
8. Plaza, S. M., and Lamson, D. W. (2005) *Altern. Med. Rev.* **10,** 24–35
9. Price, P. A., and Baukol, S. A. (1980) *J. Biol. Chem.* **255,** 11660–11663
10. Vergnaud, P., Garnero, P., Meunier, P. J., Breart, G., Kamihagi, K., and Delmas, P. D. (1997) *J. Clin. Endocrinol. Metab.* **82,** 719–724
11. Luo, G., Ducy, P., McKee, M. D., Pinero, G. J., Loyer, E., Behringer, R. R., and Karsenty, G. (1997) *Nature* **386,** 78–81
12. Murshed, M., Schinke, T., McKee, M. D., and Karsenty, G. (2004) *J. Cell Biol.* **165,** 625–630
13. Tabb, M. M., Sun, A., Zhou, C., Grun, F., Errandi, J., Romero, K., Pham, H., Inoue, S., Mallick, S., Lin, M., Forman, B. M., and Blumberg, B. (2003) *J. Biol. Chem.* **278,** 43919–43927
14. Blumberg, B., Sabbagh, W., Jr., Juguilon, H., Bolado, J., Jr., van Meter, C. M., Ong, E. S., and Evans, R. M. (1998) *Genes Dev.* **12,** 3195–3205
15. Xie, W., Barwick, J. L., Simon, C. M., Pierce, A. M., Safe, S., Blumberg, B., Guzelian, P. S., and Evans, R. M. (2000) *Genes Dev.* **14,** 3014–3023
16. Xie, W., Barwick, J. L., Downes, M., Blumberg, B., Simon, C. M., Nelson, M. C., Neuschwander-Tetri, B. A., Brunt, E. M., Guzelian, P. S., and Evans, R. M. (2000) *Nature* **406,** 435–439
17. Livak, K. J., and Schmittgen, T. D. (2001) *Methods (San Diego)* **25,** 402–408
18. Bhalla, S., Ozalp, C., Fang, S., Xiang, L., and Kemper, J. K. (2004) *J. Biol. Chem.* **279,** 45139–45147
19. Tullberg-Reinert, H., and Jundt, G. (1999) *Histochem. Cell Biol.* **112,** 271–276
20. Geick, A., Eichelbaum, M., and Burk, O. (2001) *J. Biol. Chem.* **276,** 14581–14587
21. Ohta, K., Lupo, G., Kuriyama, S., Keynes, R., Holt, C. E., Harris, W. A., Tanaka, H., and Ohnuma, S. (2004) *Dev. Cell* **7,** 347–358
22. Wiberg, C., Klatt, A. R., Wagener, R., Paulsson, M., Bateman, J. F., Heinegard, D., and Morgelin, M. (2003) *J. Biol. Chem.* **278,** 37698–37704
23. Ogushi, T., Takahashi, S., Takeuchi, T., Urano, T., Horie-Inoue, K., Kumagai, J., Kitamura, T., Ouchi, Y., Muramatsu, M., and Inoue, S. (2005) *Cancer Res.* **65,** 3700–3706
24. Bailey, A. J., Wotton, S. F., Sims, T. J., and Thompson, P. W. (1993) *Connect. Tissue Res.* **29,** 119–132
25. Schonherr, E., Witsch-Prehm, P., Harrach, B., Robenek, H., Rauterberg, J., and Kresse, H. (1995) *J. Biol. Chem.* **270,** 2776–2783
26. Mizuno, M., Fujisawa, R., and Kuboki, Y. (1996) *Calcif. Tissue Int.* **59,** 163–167
27. Mansson, B., Wenglen, C., Morgelin, M., Saxne, T., and Heinegard, D. (2001) *J. Biol. Chem.* **276,** 32883–32888
28. Waddington, R. J., Roberts, H. C., Sugars, R. V., and Schonherr, E. (2003) *Eur. Cell Mater.* **6,** 12–21
29. Xu, T., Bianco, P., Fisher, L. W., Longenecker, G., Smith, E., Goldstein, S., Bonadio, J., Boskey, A., Heegaard, A. M., Sommer, B., Satomura, K., Dominguez, P., Zhao, C., Kulkarni, A. B., Robey, P. G., and Young, M. F. (1998) *Nat. Genet.* **20,** 78–82
30. Corsi, A., Xu, T., Chen, X. D., Boyde, A., Liang, J., Mankani, M., Sommer, B., Iozzo, R. V., Eichstetter, I., Robey, P. G., Bianco, P., and Young, M. F. (2002) *J. Bone Miner. Res.* **17,** 1180–1189
31. Deak, F., Piecha, D., Bachrati, C., Paulsson, M., and Kiss, I. (1997) *J. Biol. Chem.* **272,** 9268–9274
32. Piecha, D., Muratoglu, S., Morgelin, M., Hauser, N., Studer, D., Kiss, I., Paulsson, M., and Deak, F. (1999) *J. Biol. Chem.* **274,** 13353–13361
33. Piecha, D., Wiberg, C., Morgelin, M., Reinhardt, D. P., Deak, F., Maurer, P., and Paulsson, M. (2002) *Biochem. J.* **367,** 715–721
34. Wright, S. D., Ramos, R. A., Tobias, P. S., Ulevitch, R. J., and Mathison, J. C. (1990) *Science* **249,** 1431–1433
35. Filipp, D., Alizadeh-Khiavi, K., Richardson, C., Palma, A., Paredes, N., Takeuchi, O., Akira, S., and Julius, M. (2001) *Proc. Natl. Acad. Sci. U. S. A.* **98,** 603–608
36. Manabe, N., Kawaguchi, H., Chikuda, H., Miyaura, C., Inada, M., Nagai, R., Nabeshima, Y., Nakamura, K., Sinclair, A. M., Scheuermann, R. H., and Kuro-o, M. (2001) *J. Immunol.* **167,** 2625–2631
37. Roman-Roman, S., Garcia, T., Jackson, A., Theilhaber, J., Rawadi, G., Connolly, T., Spinella-Jaegle, S., Kawai, S., Courtois, B., Bushnell, S., Auberval, M., Call, K., and Baron, R. (2003) *Bone (N.Y.)* **32,** 474–482
38. Kay, R., Rosten, P. M., and Humphries, R. K. (1991) *J. Immunol.* **147,** 1412–1416

Available online at www.sciencedirect.com
SCIENCE DIRECT
ELSEVIER
Biochemical and Biophysical Research Communications 339 (2006) 99–106
BBRC
www.elsevier.com/locate/ybbrc

Identification of novel steroid target genes through the combination of bioinformatics and functional analysis of hormone response elements

Kuniko Horie-Inoue [a], Kenichi Takayama [a,b], Hidemasa U. Bono [c], Yasuyoshi Ouchi [b], Yasushi Okazaki [c], Satoshi Inoue [a,b,*]

[a] *Division of Gene Regulation and Signal Transduction, Research Center for Genomic Medicine, Saitama Medical School, 1397-1 Yamane, Hidaka-shi, Saitama 350-1241, Japan*
[b] *Department of Geriatric Medicine, Graduate School of Medicine, The University of Tokyo, 7-3-1 Hongo, Bunkyo-ku, Tokyo 113-8655, Japan*
[c] *Division of Functional Genomics and Systems Medicine, Research Center for Genomic Medicine, Saitama Medical School, 1397-1 Yamane, Hidaka-shi, Saitama 350-1241, Japan*

Received 18 October 2005
Available online 8 November 2005

Abstract

Steroid hormone receptors including androgen receptor (AR), glucocorticoid receptor (GR), progesterone receptor (PR), and mineralocorticoid receptor (MR) recognize and bind to identical consensus hormone response elements (HREs), which consist of two hexameric half-sites (5′-AGAACA-3′) arranged as inverted repeats with a 3-bp spacer. Although only a few near-consensus HRE sequences have been identified in the transcriptional regulatory regions of known steroid target genes, it has been unclear whether the exact consensus sequences function as bona fide HREs in vivo. A genome-wide in silico screening of palindromic HREs identified 565 exact consensus sequences in human genome (NCBI 35 assembly). In this study, of 565 exact consensus elements, functional in vivo receptor binding was evaluated regarding 26 sequences located within 10 kb upstream to the 5′ end of annotated genes through chromatin immunoprecipitation (ChIP) assay using cells endogenously expressing steroid hormone receptors. Hormone responsiveness of proximal gene expression was examined through quantitative RT-PCR. As far as performing ChIP assay for AR, GR, and PR, 14 of 26 elements significantly recruited at least one of the receptors by hormone treatment (>2-fold enrichment versus vehicle). In terms of gene expression in the vicinity of the above 14 functional perfect HREs, four genes were upregulated by >2-fold with hormone treatment. The present data suggest that the combination of bioinformatics analysis and quantitative experimental evaluation is useful to identify novel functional HREs that may contribute to the transcriptional regulation of steroid target genes.

Keywords: Androgen receptor; Progesterone receptor; Glucocorticoid receptor; Steroid target gene; Hormone response element; Chromatin immunoprecipitation; Quantitative PCR; Transcriptional start site

Steroid hormone receptors are nuclear receptors that play essential roles in various physiological and pathophysiological states. Forming complexes with coactivators and general transcription factors, ligand-stimulated steroid hormone receptors including androgen receptor (AR), glucocorticoid receptor (GR), progesterone receptor (PR), and mineralocortitoid receptor (MR) recognize and bind to hormone response elements (HREs) in the regulatory regions of various hormone responsive genes, leading to the modulation of target gene transcription [1]. Despite the degeneracy of the nucleotide sequence of the HREs, steroid hormone receptors generate distinct hormone-specific responses. The palindromic 15-bp sequence (5′-AGAACA*nnn*TGTTCT-3′) that contains inverted repeats with a 3-bp spacer (IR3 sequence) has been identified as the consensus sequence for HRE [2], though only a few perfect consensus HREs have yet been identified in the regulatory regions of known hormone responsive genes. A question that continues to engage the steroid receptor field is

* Corresponding author. Fax: +81 42 985 7209.
E-mail address: s_inoue@saitama-med.ac.jp (S. Inoue).

0006-291X/$ - see front matter © 2005 Elsevier Inc. All rights reserved.
doi:10.1016/j.bbrc.2005.10.188

whether perfect HRE sequences function as hormone receptor binding sites in vivo, which regulate the transcription of steroid target genes.

Previously, we have identified perfect ARE sequences of IR3 type in silico in the human genome and characterized AR-binding ability of perfect AREs on chromosome X [3]. More than one-third of perfect ARE sequences (8 of 21) recruited more ARs compared with the proximal promoter region of prostate-specific antigen (PSA) containing a functional ARE. In the present study, we extend our study to a question whether perfect HRE sequences in silico situated in the proximal upstream regions of annotated genes function as bona fide functional binding sites for steroid hormone receptors in human cells derived from different tissues. Our combined approach of bioinformatics and experimental validation identified several perfect HRE sequences that could bind to steroid hormone receptors and some proximal downstream genes that were responsive to hormone treatment in the vicinity of the perfect HREs.

Materials and methods

Bioinformatics. Consensus HREs in the human genome (Ensembl version 34 based on the NCBI 35 assembly retrieved from Ensembl ftp site [4]) were screened by a 'pipeline' computational system called SayaMatcher [5], which utilizes in-house Perl script and a program for regular expression search of a nucleotide sequence (program name: dreg) in EMBOSS package [6]. The regular expression pattern for HRE was obtained from a recent literature by Nelson et al. [7], in which the palindromic 5′-AGAACAnnnTGTTCT-3′ sequence corresponding to the ARE sequence in TRANSFAC database [8] was used as a consensus sequence.

Cell culture. Human prostate cancer LNCaP cells and DU145 cells, breast cancer T47D cells, and osteosarcoma SaOS2 cells were purchased from American Type Culture Collection (Rockville, MD). LNCaP cells were maintained in RPMI 1640 supplemented with 4.5 g/dl glucose, 1 mM sodium pyruvate, 10 mM Hepes, and 10% fetal bovine serum (FBS). Other cells were maintained in DMEM supplemented with 10% fetal bovine serum (FBS). Prior to hormone addition, cells were cultured for 2 days in phenol red-free RPMI 1640 or DMEM supplemented with 5% dextran-charcoal stripped FBS (dcc-FBS) and 1 day in phenol red-free medium supplemented with 2.5% dcc-FBS.

Chromatin immunoprecipitation assay. Chromatin immunoprecipitation (ChIP) assay was performed as described previously [3]. LNCaP cells, T47D cells, and DU145 cells as well as SaOS2 cells after 72-h hormone depletion were treated with 10 nM R1881 (NEN Life Science Products, Boston, MA), progesterone (Sigma), or dexamethasone (Sigma), respectively, for indicated times. Control cells were treated with 0.1% ethanol as a vehicle. Cells were fixed in 1% formaldehyde for 5 min at room temperature. Chromatin was sheared to an average size of 500 bp by sonication using a Bioruptor ultrasonicator (Cosmo-Bio, Tokyo, Japan). Lysates corresponding to 2×10^7 cells were rotated at 4 °C for overnight with 3 μg of polyclonal antibodies against AR (H-280, Santa Cruz Biotechnology, Santa Cruz, CA), PR (H-190, Santa Cruz Biotechnology), or GR (H-300, Santa Cruz Biotechnology). Salmon sperm DNA/protein A–agarose (Upstate Biotechnology, Lake Placid, NY) was added and incubated for 1 h. Washing and reversal of cross-links was performed as described [9]. Precipitated DNA fragments were quantified by quantitative real-time PCR using the Applied Biosystems 7000 sequence detector (Foster City, CA) based on SYBR Green I fluorescence. Primer pairs were designed by Primer Express ver. 2.0 software (Applied Biosystems), generating perfect ARE-containing fragments with the requirements of primer T_m temperature at basically 58–60 °C and the requirements of amplicon length for 50–150 bp. The protocol of PCR was 2 min at 50 °C, 10 min at 95 °C, and 40 cycles of 15 s at 95 °C and 1 min at 60 °C. To determine relative differences among the treatment groups for the ChIP assays, we used the $\Delta\Delta C_T$ method as outlined in the Applied Biosystems protocol for reverse transcriptase-PCR (http://www.appliedbiosystems.com/). The threshold cycle C_T was defined as the cycle at which the fluorescence signal was statistically significant over background. The reciprocal of 2^{C_T} (used C_T as an exponent for the base 2) for each target element was normalized by that for an external control of the genomic fragment GAPDH and subsequently normalized by input DNAs obtained from either steroid or vehicle-treated cells. Fold enrichment in steroid-treated cells was obtained through the division by the values in vehicle-treated cells. Genomic fragments containing proximal or distal ARE in the promoter region of prostate-specific antigen (PSA) [−250 to −39 bp and −4170 to −3978 bp from the transcriptional initiation site (TSS), respectively] [3,9] were used as positive controls for AR binding. The proximal promoter region of α subunit of amiloride-sensitive epithelial sodium channel (ENaCα) (−867 to −761 bp from the TSS, containing the GRE sequence as previously described [10]) was used as a positive control for GR binding. We also used a genomic fragment on the intron 1 of FK506 binding protein 51 (FKBP51) (+359 to +426 bp from the TSS of the long isoform ENST00000357266) as a positive control for GR and PR binding, which was newly identified in our ChIP assay scanning the gene regulatory region of FKBP51. The quality of precipitated DNA was analyzed by PCR amplification of positive controls and 8% polyacrylamide electrophoresis prior to quantitative analyses and the batches of ChIP samples with maximal responses were selected for quantitative PCR. The sequences of the primers used in ChIP assays (synthesized by Sigma Genosys, Japan) are described in Table 1.

Quantitative reverse transcription-PCR. Total RNA was extracted from hormone-treated or 0.1% ethanol-treated cells for indicated times using ISOGEN reagent (Nippon Gene, Tokyo, Japan). First strand cDNA was generated from RNase-free DNase I-treated total RNA by using SuperScript II Reverse Transcriptase (Invitrogen, Carlsbad, CA) and pdT_{12-18} primer (Amersham Biosciences, Piscataway, NJ). Hormone responsiveness of the proximal genes located downstream to the 26 perfect HRE sequences was analyzed by quantitative reverse transcription-PCR (RT-PCR) using the Applied Biosystems 7000 sequence detector based on SYBR Green I fluorescence. Primer design and PCR protocol were as described above. The evaluation of relative differences of PCR product amounts among the treatment groups was carried out using the $\Delta\Delta C_T$ method. The reciprocal of 2^{C_T} (used C_T as an exponent for the base 2) for each target gene was normalized by that for GAPDH coding region, followed by the comparison with the relative value in vehicle-treated cells. PSA was served as a positive control for androgen responsiveness, while FKBP51 was used for both progesterone and glucocorticoid responsiveness. ENaCα was another positive control for the glucocorticoid response and the progesterone-dependent change of ENaCα mRNA level was also evaluated. The primer sequences for the amplifications are described in Table 2.

Results

In silico identification of perfect palindromic HRE sequences in the human genome

In terms of palindromic HRE sequences composed of two AGAACA sequences separated by a 3-bp spacer, only a few near-consensus sequences have been identified in the vicinity of human genes that are responsive to steroid hormones including androgen, progesterone, glucocorticoid, and mineralocorticoid. In order to answer the question of whether perfect palindromic HRE sequences do function as in vivo binding sites for steroid hormone receptors, we computationally searched for all the consensus HRE sequences in the human genome utilizing in-house Perl

Table 1
Primers for quantitative ChIP assay

Target	Forward primer	Reverse primer
HRE sites		
HRE1	5′-CCAAATATGTCCATTCATCCAACA-3′	5′-GGAAACATACGCATTGCCTAGAA-3′
HRE2	5′-CCAACAAACACTAGCAGAACATTATG-3′	5′-AGAGGGCATCTGAACAATAGAAGA-3′
HRE3	5′-CAAGGCCTGGGGACATTTAA-3′	5′-CGAAGCTGCTGGGAGGTATC-3′
HRE4	5′-TCAAAGGTGGTGCTTATCAT-3′	5′-GAACTGAGTTCCAGGAAATATG-3′
HRE5	5′-AAGGGAAAAGATCTCATATTGCA-3′	5′-CACGGCAATTTTAATACTCATCA-3′
HRE6	5′-GACCATACCTTGGTATGACCCCTT-3′	5′-TCTGTGGTTATCCTGCAAGTCAGT-3′
HRE7	5′-AAGAAACCATTTTGAAATGTGCC-3′	5′-CAGGTCAGTTAGGCTCTGATAAAACC-3′
HRE8	5′-TACTTACCCAGTGCTTCCCAATC-3′	5′-GAGCACCTGAGGTGTTTTTTTT-3′
HRE9	5′-AGCGAGACTCCGTCTTAAA-3′	5′-GGAGGAGTTACTGTTACAATTAT-3′
HRE10	5′-ACACTGTGGTGGGCAGGATT-3′	5′-GCTCAAACAAACAGGCTAAGACA-3′
HRE11	5′-TGTCCTTCTGAAGACTTCCATTCC-3′	5′-TACAGGCACACACCACCAGATTG-3′
HRE12	5′-CTTGCAGTGAGCCGAGATC-3′	5′-TTCTGGAGGAGTTACTGTTACAATTA-3′
HRE13	5′-CCTGCTCTTTGATTTTCGTAAGA-3′	5′-TGAAGCCAAATGCTGAAGTG-3′
HRE14	5′-TTGACAGTATATTTAGAGCGTGTTATCT-3′	5′-GTTAATTCTCTTTCCCTATGGTAGAAT-3′
HRE15	5′-TGTGCAAGAAATGCCATCCT-3′	5′-CATCATAGCTGCATGGGTGTT-3′
HRE16	5′-TGAAAATAATTTCACTTATCCTTTAAGC-3′	5′-AATGACTTGCTGACCAAATCC-3′
HRE17	5′-GGCCTATTTTAATCAGCATTTCAGA-3′	5′-ATCCTCATTCCTACCCAGCATCT-3′
HRE18	5′-ACATCAGTGGCTCTTAAGCACTG-3′	5′-CAGAGAGAATAAAAAAACTAGCCCAAA-3′
HRE19	5′-AATGCTGCTCAAAGAAATCAGA-3′	5′-TTTAATTCCAAATGCATTTTAGAAC-3′
HRE20	5′-CTCCATGTTTGAGGCGGAGA-3′	5′-CATCCCACTTTGTGCGTAACTTT-3′
HRE21	5′-CTCCAGGGCTGTACTGGTATCTG-3′	5′-CAGGTGTGGGCCCTCTGT-3′
HRE22	5′-TCTTAAGCAAAAGGCCAACAA-3′	5′-TCTATCATTACAAGAAAAGTTGGTTATCTG-3′
HRE23	5′-GCCAGCACTCACGTGGCTAT-3′	5′-CTGCGGTGCCGTGACA-3′
HRE24	5′-TGTACACACAAAAACTGCTAGAACACTCT-3′	5′-GCTCAGCCATGGGTTGGT-3′
HRE25	5′-GGGAGCTGGCTAGAACACTCA-3′	5′-CATGCTGGGCTAAAGCAGAAC-3′
HRE26	5′-TGTGTGCTCAAAGAGTAGATTGG-3′	5′-TCATCACTTATTGCCTGAACTATCA-3′
FKBP51 intron 1	5′-TGCAAGAGCGGTTGATCTG-3′	5′-GCGAGAACAGCCTGACTCA-3′
ENaCα promoter	5′-CCTCTGGTTGCCCACATTC-3′	5′-GGGCCCTAGGACATTCTGTT-3′
PSA proximal promoter	5′-TCTGCCTTTGTCCCCTAGAT-3′	5′-AACCTTCATTCCCCAGGACT-3′
PSA distal promoter	5′-ACAGACCTACTCTGGAGGAAC-3′	5′-AAGACAGCAACACCTTTTT-3′

script and a program for regular expression pattern search of a nucleotide sequence in the EMBOSS package (program name: dreg) as previously described [3,5]. The screening defined 563 sequences on the NCBI 34 assembly of the human genome [3] and additional two sites on the NCBI 35 assembly. The two new sequences were located on chromosomes 1 and 14. The number of HRE sites was larger than the expected frequency in random DNA sequences as calculated by the total number of base pairs in the genome devided by the frequency of a sequence with specific base pairs at 12 positions ($3272\ \text{Mb}/4^{12} = 195$). The distribution of consensus sequences among the chromosomes is generally consistent with chromosomal size [3]. The highest frequency of HRE was 28.0 sites per 100 Mb on chromosome 8 and the lowest frequency was 6.9 sites per 100 Mb on chromosome Y, the average being 17.4 ± 4.4 sites per 100 Mb.

Perfect HREs located in the proximal upstream regions of annotated genes

To investigate whether the computationally identified perfect HRE sequences located in the canonical proximal promoters of annotated genes particularly function as steroid hormone receptor binding sites, we selected perfect HREs lying within 10 kb upstream to the transcriptional start sites (TSSs) of known human genes on the Ensembl Genome Browser [4]. We obtained 26 of 565 perfect HRE sequences (4.6%) in the proximal promoter regions of annotated genes (Table 3). The distribution of 26 perfect HREs in the proximal promoter elements was limited to 14 of 24 chromosomes and rather independent of chromosomal size. The longest chromosome 1 contained 5 sequences, while 4 sequences were found in both chromosomes 6 and 11.

In vivo recruitment of steroid hormone receptors to perfect HREs located 5′ to annotated genes

To assess whether these perfect HREs situated within 10 kb of the 5′ ends of known genes (5′ HREs) do recruit steroid hormone receptors in vivo, we performed ChIP assay in human cells endogenously expressing receptors. Hormone-depleted cells were treated for 24 h (also 2 h in T47D cells) with either 10 nM of steroids or 0.1% ethanol as a vehicle, cross-linked by formaldehyde, sonicated, and immunoprecipitated by specific polyclonal antibodies against steroid receptors. LNCaP cells were treated with R1881 (or vehicle) and immunoprecipitated by AR antibody; T47D cells were treated with progesterone and immunoprecipitated by PR antibody; and DU145 cells as well as SaOS cells were treated with dexamethasone and

Table 2
Primers for quantitative RT-PCR

Target	Adjacent HRE	Forward primer	Reverse primer
IQSEC2	HRE1	5′-ACATCACAGAACTTGAGGACTCCTT-3′	5′-AGGGCTTCGTCGATGGATTC-3′
MELL1	HRE2	5′-GAGATCACGCACGGCTTTG-3′	5′-CCAATCCATCATGTTGCCATT-3′
HS163_HUMAN	HRE3	5′-GATGGAGGCGGTGGTGTTC-3′	5′-GTAATTATGAAGTAGACCGAGAGGAAGAT-3′
DISP1	HRE4	5′-CATGGAGCTGGAAAGGAGTACAG-3′	5′-CACCACTGCCCTGATAGTATCATT-3′
EXTL2	HRE5	5′-AGGCAGCCACGTGTTCTATTG-3′	5′-TTAACGCAGCAAAACGATCACT-3′
NP_689710.1	HRE6	5′-GAGGGCAGTGGCGTGATC-3′	5′-CAGTAGAATGGCGTGAACTCAGA-3′
B3GALT3	HRE7	5′-TGCAGCCCATGGCTTTTC-3′	5′-GGCATGTGGTGTTCCTTAGCA-3′
SLC36A1	HRE8	5′-CGGAAGGCCTCAACAACCT-3′	5′-CCATGTTGTGCTATTGCTTTGAC-3′
DAXX	HRE9	5′-GCCCTTCACCACTGTCTTAGAGA-3′	5′-GAGACGCCTCCATTGAAGGA-3′
ULBP3	HRE10	5′-CGGACTGACCACCTTCTTCAA-3′	5′-TGCATCAGGAAGTCCCTAAGC-3′
KIF13A	HRE11	5′-GCTGCTATGGAGTTAGTATTACGAAAAC-3′	5′-CTTCAAACTCTGCGTGAAACTCTGT-3′
ZNF297	HRE12	5′-CCTCTCAAGGATGCGCTCTT-3′	5′-GGGAATTTCCACGGGAAGTC-3′
GIMAP5	HRE13	5′-CAGGTGAAAACAGGAACATGGA-3′	5′-GGCCTGTGACTCAAAGATGGA-3′
ZNF398	HRE14	5′-GAGCTTCCGCTACAAACAGACA-3′	5′-ACCCCCACAGCCTCCATT-3′
NP_055096.2	HRE15	5′-CAGTGACCTCTCTGCGTGACA-3′	5′-AACCCAGAGGAAACAAGGAACA-3′
Q9C0D7_HUMAN	HRE16	5′-CCAGCTGTCCTGGCGACTAC-3′	5′-AGTCGAGAGTCAGAGATGCTGTCTATT-3′
OR8D4	HRE17	5′-GCTTTTATCCTCACCAGCATCCT-3′	5′-GAGCTACAGGTGCTAAACGCTTT
ENSG00000182203	HRE18	5′-ACACCAACAGGATACACTGAAAGC-3′	5′-GCACATTTAACTTGCAGGTTTTTG-3′
ENSG00000185439	HRE19	5′-TGCCTTCATGGTGGACAATG-3′	5′-GGATGCTCGATGTCCAGGTT-3′
CV106_HUMAN	HRE20	5′-CACAATTTAACTTACGAACTTCCAACTC-3′	5′-GCCAACTGAGCTCTAGTTAATGTCTTG-3′
SRP14	HRE21	5′-GTTGTTGGAGAGCGAGCAGTT-3′	5′-CCGACGTCCGGCACTTC-3′
NP_874362.2	HRE22	5′-TGCAGCGACTTGTGGACATC-3′	5′-CGAATGCAGGGCAGTCAGA-3′
MVD	HRE23	5′-TGGCGGCAGTCACTTGTACA-3′	5′-CGCGCTTGCCCCAGTA-3′
ENSG00000189289	HRE24	5′-GCCTGCTCCACCCAGAGAA-3′	5′-AACAGGTTCCAGCAGCTCAGA-3′
NP_775751.1	HRE25	5′-CACCAAGTGCAGGACAGTCTTC-3′	5′-GGTGCTTTTCGTCCACAGTGA-3′
NP_689725.2	HRE26	5′-CTTTACTAGCAACACCTCCTTCCAT-3′	5′-TGCACCCGAAAGATTACAAACTT-3′
FKBP51 coding		5′-CTGCAGAGATGTGGCATTCACT-3′	5′-TCCAGAGCTTTGTCAATTCCAA-3′
ENaCα coding		5′-CGCATGAAGACGGCCTTCT-3′	5′-CGCATGAAGACGGCCTTCT-3′
PSA coding		5′-GCCCTGCCCGAAAGG-3′	5′-GATCCACTTCCGGTAATGCA-3′
GAPDH coding		5′-GGTGGTCTCCTCTGACTTCAACA-3′	5′-GTGGTCGTTGAGGGCAATG-3′

Table 3
Perfect HRE sites that locate upstream to annotated genes at a distance within 10 kb

HRE ID	Chr. location	Start position	Stop position	HRE sequence	Proximal gene	Ensembl ID	Distance (kb)
HRE1	Xp11.22	53237415	53237429	AGAACAttaTGTTCT	IQSEC2	ENSG00000124313	3.9
HRE2	1p36.32	2603985	2603999	AGAACAagcTGTTCT	MELL1	ENSG00000142606	7.4
HRE3	1q42.12	220841360	220841374	AGAACAgttTGTTCT	HS163_HUMAN	ENSG00000143771	9.9
HRE4	1q41	219495172	219495186	AGAACAgtaTGTTCT	DISP1	ENSG00000154309	9.4
HRE5	1p21.1	101079768	101079782	AGAACAtaaTGTTCT	EXTL2	ENSG00000162694	6.2
HRE6	1p36.11	25913162	25913176	AGAACAgctTGTTCT	NP_689710.1	ENSG00000177493	9.9
HRE7	3q26.1	162310806	162310820	AGAACAttcTGTTCT	B3GALT3	ENSG00000169255	5.0
HRE8	5q33.1	150798127	150798141	AGAACAggcTGTTCT	SLC36A1	ENSG00000123643	9.2
HRE9	6p21.32	33401650	33401664	AGAACAttcTGTTCT	DAXX	ENSG00000007565	3.0
HRE10	6q25.1	150487454	150487468	AGAACAataTGTTCT	ULBP3	ENSG00000131019	5.1
HRE11	6p22.3	18101058	18101072	AGAACAtgcTGTTCT	KIF13A	ENSG00000137177	5.4
HRE12	6p21.32	33401650	33401664	AGAACAttcTGTTCT	ZNF297	ENSG00000168351	8.2
HRE13	7q36.1	149868965	149868979	AGAACAcaaTGTTCT	GIMAP5	ENSG00000196329	3.2
HRE14	7q36.1	148274989	148275003	AGAACAttaTGTTCT	ZNF398	ENSG00000197024	7.5
HRE15	8q24.3	144987498	144987512	AGAACAccgTGTTCT	NP_055096.2	ENSG00000179950	8.9
HRE16	11q22.3	109509863	109509877	AGAACAtttTGTTCT	Q9C0D7_HUMAN	ENSG00000149289	1.9
HRE17	11q24.1	123276891	123276905	AGAACAaagTGTTCT	OR8D4	ENSG00000181518	5.5
HRE18	11q24.2	125433385	125433399	AGAACAaaaTGTTCT	ENSG00000182203	ENSG00000182203	9.3
HRE19	11q12.3	62569237	62569251	AGAACAaatTGTTCT	ENSG00000185439	ENSG00000185439	1.8
HRE20	14q21.2	44792647	44792661	AGAACAtttTGTTCT	CV106_HUMAN	ENSG00000129534	0.5
HRE21	15q15.1	38128202	38128216	AGAACAaacTGTTCT	SRP14	ENSG00000140319	9.5
HRE22	15q22.3	62987265	62987279	AGAACAgatTGTTCT	NP_874362.2	ENSG00000166839	3.9
HRE23	16q24.3	87266241	87266255	AGAACAacttGTTCT	MVD	ENSG00000167508	9.2
HRE24	17q21.32	44836359	44836373	AGAACActcTGTTCT	ENSG00000189289	ENSG00000189289	3.2
HRE25	19p13.3	2844818	2844832	AGAACAggaTGTTCT	NP_775751.1	ENSG00000171970	7.1
HRE26	22q13.1	38616692	38616706	AGAACAgaaTGTTCT	NP_689725.2	ENSG00000176177	2.4

immunoprecipitated by GR antibody. We performed quantitative PCR using the genomic DNA obtained from each cell line (Fig. 1). The proximal and distal promoter regions of PSA including ARE sequences were used as positive controls for the AR association [3], and the proximal promoter of ENaCα including HRE sequences [10] was used as a positive control for the GR. The proximal promoter fragment of ENaCα was also found to recruit PR in the present study, as the PR recruitment to the fragment was ~9.5- and ~20-fold versus vehicle by 2 and 24-h treatments, respectively (Fig. 1B). FKBP51 has been previously described as a glucocorticoid or progesterone-inducible gene [11,12], however, functional HREs in the gene regulatory region have not been well characterized. We newly identified a functional HRE in the intron 1 of FKBP51 through scanning the gene regulatory region by ChIP assay. The intronic HRE of FKBP51 recruited PR in T47D cells as well as GR in DU145 cells and SaOS2 cells (Figs. 1B–D).

Of 26 genomic fragments containing perfect 5′ HRE sequences, 14 fragments recruited either one of the three steroid receptors by >2-fold enrichment in steroid-treated cells versus vehicle-treated cells (Fig. 1). HRE20 recruited three different receptors while HRE1, HRE15, and HRE24 recruited two different receptors by >2-fold enrichment. Other HRE sequences preferentially bound to only one steroid receptor. There seems to be no particular specificity of 3-bp spacer sequences for the receptor recruitment among the 14 functional HRE sequences.

Potential transcriptional regulation of proximal genes located downstream to perfect HREs

To examine whether the functional perfect 5′ HREs regulate transcriptional activity of their downstream proximal genes, we next performed quantitative RT-PCR for the downstream genes in the vicinity of the functional perfect 5′ HRE sequences. Of 7 proximal genes in the vicinity of functional perfect 5′ HRE sequences that recruited AR by >2-fold enrichment in LNCaP cells, OR8D4 (olfactory receptor family 8, subfamily D, member 4) adjacent to HRE17 exhibited a >2-fold increase in the mRNA level androgen-dependently (Fig. 2A). Of nine proximal genes in the vicinity of functional perfect 5′ HREs in T47D cells, MELL1 (mel transforming oncogene-like 1) and NP_775751.1 adjacent to HRE2 and HRE25, respectively, were upregulated by >2-fold at the mRNA level by progesterone treatment (Fig. 2B). Neither gene adjacent to the 2 functional perfect 5′ HREs in DU145 cells exhibited >2-fold increase in mRNA level, whereas Q9C0D7 adjacent to HRE16 in SaOS2 cells was upregulated by >2-fold at mRNA level glucocorticoid-dependently (Figs. 2C and D).

Discussion

A genome-wide in silico screening of palindromic perfect HREs identified 565 exact consensus sequences in the NCBI 35 assembly of the human genome. Of 565 perfect HRE sequences, 26 sites were situated within 10 kb upstream to the TSS of annotated genes. We investigated whether these perfect 5′ HRE sequences functioned as bona fide binding sites for steroid hormone receptors in different cell lines, and demonstrated that 14 of 26 perfect HREs significantly (>2-fold) recruited some of the receptors by performing ChIP assay for AR, GR, and PR binding. Hormone-dependent upregulation of mRNA level by >2-fold was shown in the four proximal genes adjacent to the functional perfect 5′ HREs. The average distance between 5′ HREs and the TSS of their proximal genes was not significantly smaller among these four proximal genes compared with the all 26 proximal genes in the vicinity of perfect 5′ HREs; the former and latter values were 4.5 ± 2.4 and 6.0 ± 3.0 kb, respectively.

The four hormone-responsive proximal genes adjacent to functional 5′ HRE sequences were upregulated by only either one of the three steroid hormone receptors and not by two or three other receptors. OR8D4 (HRE17) was identified as an AR target gene in LNCaP cells, MELL1 (HRE2) and NP_775751.1 (HRE25) were identified as PR target genes in T47D cells, and Q9C0D7 (HRE 16) was identified as a GR target gene in SaOS2 cells. Although a single IR3 type consensus HRE may be a potential binding site for various steroid hormone receptors, no common target gene for AR, PR, and GR was identified among the proximal genes close to the functional perfect 5′ HREs by the functional criteria used in this study. It is also notable that no significant GR target gene was shown in DU145 cells up to 24-h dexamethasone treatment, though the mRNA level of NP_055096.2 (HRE15) was increased >2-fold by 48-h treatment (data not shown). The results of DU145 and SaOS2 cells suggest that target genes for even a single steroid hormone receptor may be varied in different cell systems. Future studies including such as the chromosomal accessibility, the receptor recognition mechanism, and the coactivator recruitment in the surroundings of consensus HREs may reveal the specificity and the similarity of the transcription factor binding sites.

Besides the functions of the above four perfect HRE sequences adjacent to the steroid target genes, other near-consensus HRE sequences may participate in the regulation of gene expression. Using the SayaMatcher system [5] that enables us to visualize the genomic position for HREs on the Ensembl browser, we found several other near-consensus HRE sequences (>80% relative profile score threshold) based on the position-specific scoring matrix for ARE (MA0007) on the Jaspar database (http://jaspar.cgb.ki.se/), which is a collection of transcription factor DNA-binding preferences [13]. For instance, there is a near-consensus HRE at ~8-kb downstream to the 3′-end of MELL1. In the vicinity of Q9C0D7, one near-consensus HRE is in the intron 1 and the other is situated at 40-kb downstream to the 3′-end. OR8D4 contains a near-consensus HRE in its only exon. Although no particular high score position for the ARE matrix is found in the vicinity of NP_775751.1, there are a number of nuclear

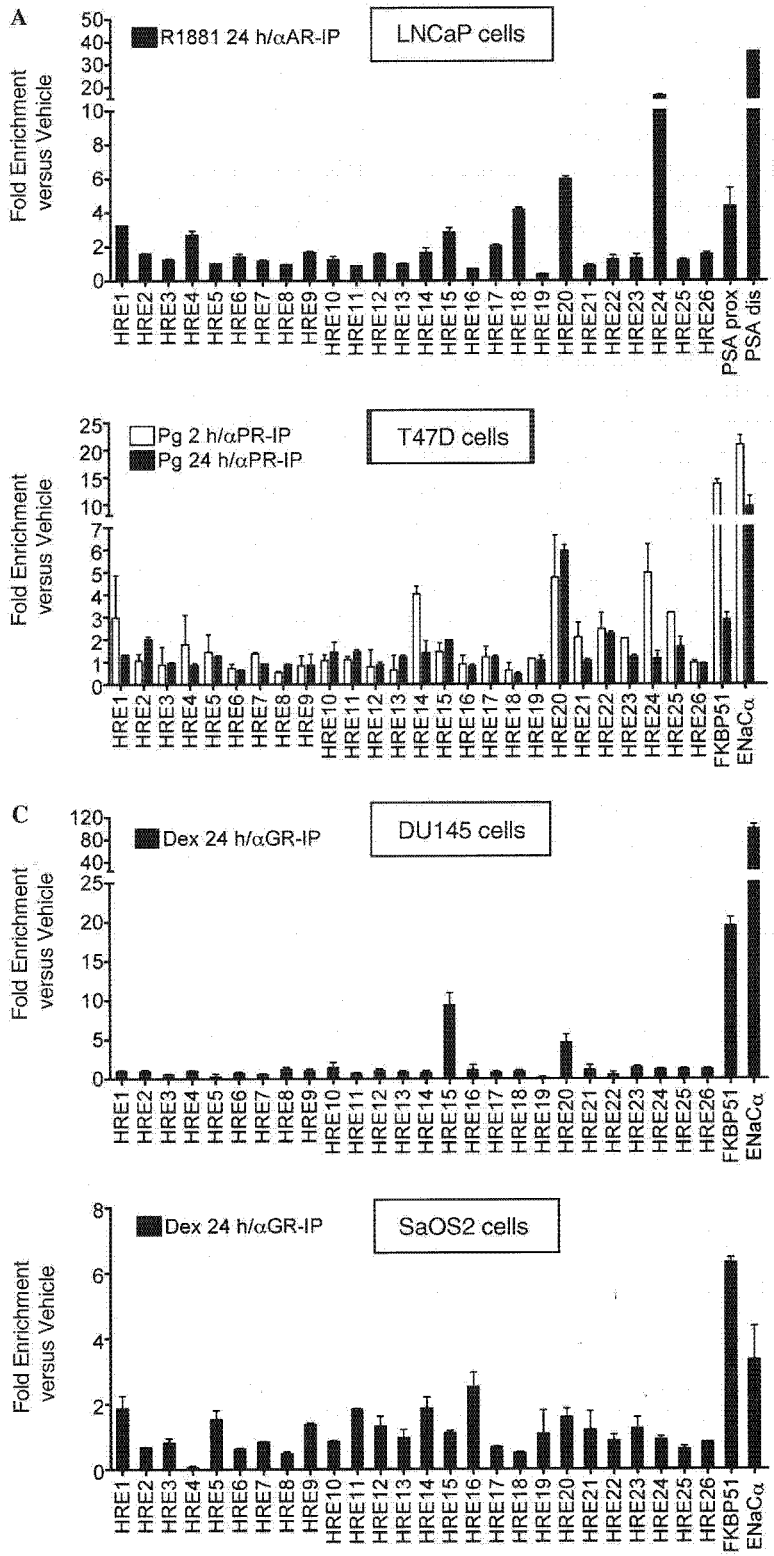

Fig. 1. In vivo recruitment of steroid hormone receptors to perfect HREs in the proximal upstream region of annotated genes. LNCaP, T47D, DU145, and SaOS2 cells after 72-h hormone depletion were treated with indicated hormones (10 nM each) or vehicle (0.1% EtOH) for indicated times. Immunoprecipitated DNA fragments were quantified by quantitative real-time PCR. In each case, fold enrichment values in hormone-treated samples precipitated by specific antibodies against receptors were normalized by those in vehicle-treated samples precipitated by the identical antibodies. Each result is the mean ± SD of two independent experiments in duplication (four determinants). Prostate-specific antigen (PSA) proximal (prox) and distal (dis) promoter regions including HREs were used as positive controls for AR binding. FK506-binding protein, 51-kDa (FKBP51) intron 1, and epithelial sodium channel α subunit (ENaCα) proximal promoter regions were used as positive controls for PR and GR binding. (A) AR recruitment in prostate cancer LNCaP cells. (B) PR recruitment in breast cancer T47D cells. (C) GR recruitment in prostate cancer DU145 cells. (D) GR recruitment in osteosarcoma SaOS2 cells.

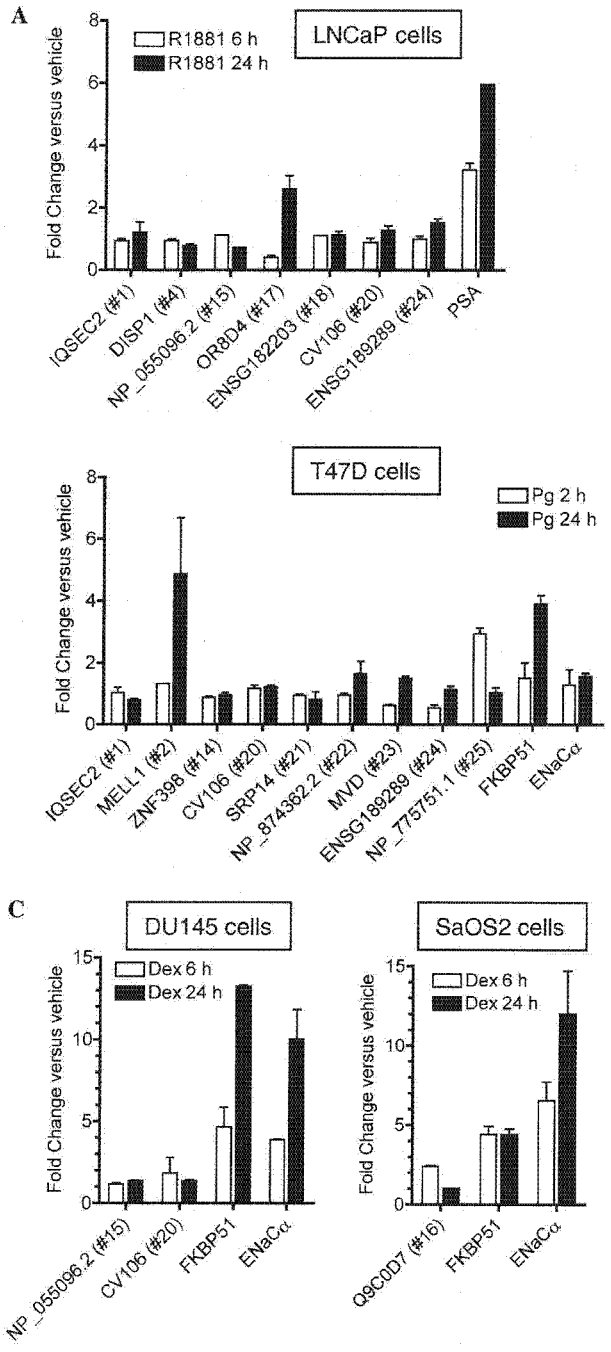

Fig. 2. Quantitative RT-PCR of proximal genes downstream to perfect HREs. LNCaP, T47D, DU145, and SaOS2 cells after 72-h hormone depletion were treated with indicated hormones (10 nM each) or vehicle (0.1% EtOH) for indicated times. Real-time PCR was conducted using the first strand cDNAs generated from the total RNAs of these cells. Each result is the mean ± SD of two independent experiments in duplication (four determinants). PSA was served as a positive control for androgen responsiveness. FKBP51 and ENaCα were served as positive controls for progesterone and glucocorticoid responsiveness. The numbers in parentheses after annotations correspond to the HRE ID in the vicinity of target genes. (A) R1881-dependent gene expression in LNCaP cells. (B) Progesterone-dependent gene expression in T47D cells. (C) Dexamethasone-dependent gene expression in DU145 cells. (D) Dexamethasone-dependent gene expression in SaOS2 cells.

receptor binding sites in the surroundings of the gene, suggesting that the region may be active for transcriptional regulation. Future studies will reveal whether these near-consensus HRE sequences coordinately function with the perfect HRE in the transcriptional regulation of the proximal genes.

Regarding the new steroid target genes identified in the present study, none of the genes has been characterized in connection with steroid hormones. The AR target gene OR8D4 (UniGene Hs. 449688) encodes a putative G protein-coupled receptor that belongs to the olfactory receptor superfamily, which is the largest gene family in the mammal genomes. In the mouse genomes, ~1300 genes were identified, whereas the number of olfactory receptors is expected ~500–750 genes in human [14]. Although ligands for most of the olfactory receptors have not been identified, it is plausible that certain receptors for odors or pheromones may be regulated by sex steroid hormones including androgen. The PR target gene MELL1 (UniGene Hs. 546429) is a membrane-bound zinc metalloprotease. It has been recently shown that mouse ortholog NL1 is expressed mainly in the testis as a secreted protein and male mice deficient in the NL1 exhibited reduced fertility [15]. It seems to be an interesting question whether human MELL1 may also play a role in reproductive tissues, particularly in the organs regulated by the progesterone-mediated gene network.

Another PR target gene NP_775751.1 encodes a putative KRAB domain-containing zinc finger protein. KRAB-containing zinc finger proteins are characterized to participate in the regulation of cell differentiation and development through transcriptional repression of RNA polymerase promoters, RNA binding, and RNA splicing [16]. Although many of these proteins have been identified, little is known about their structure and function. Since NP_775751.1 is clustered with a number of KRAB-containing zinc finger proteins on 19p13.3, these KRAB-containing zinc finger proteins might have arisen from a divergence event during evolution and may function coordinately in the various developmental and differentiation stages of organs. The GR target gene Q9C0D7 in SaOS2 cells is also annotated as zinc finger CCCH-type containing 12C (UniGene Hs. 376289). The CCCH-type zinc finger proteins such as tristetraprolin has been known as a binding protein to AU-rich element containing RNA transcripts [17], though no particular function of Q9C0D7 has yet been characterized.

In the present study, we focused on the perfect HRE sequences in the proximal upstream regions of annotated genes and found some of the elements were functional binding sites for steroid hormone receptors. It has been recently revealed, however, that transcription factor binding sites in intronic regions or in the 3′ downstream regions are also important for transcriptional regulation. Indeed, half of the perfect intronic ARE sequences on chromosome X (5 of 10) recruited more ARs compared with the proximal ARE on the PSA promoter in our

previous study [3]. In this study, we found that the FKBP51 intronic HRE sequence exhibited a significant binding ability for GR and PR. In the case of transcription factor binding sites on chromosomes 21 and 22, 36% of these regions are situated within known genes or proximal to the 3′ most exon of a gene and the frequency was also higher than that of binding sites within 5′ to known genes (22%) [18]. Thus, the further characterization of HRE sequences in introns as well as 3′ downstream regions will be required to reveal the whole entity of the transcriptional regulation mechanism mediated through steroid hormone receptors.

In summary, we have presented an integrated strategy for exploring novel steroid target genes that possess a functional perfect HRE sequence in their proximal upstream regions. Our results have shown that more than half of the perfect HREs identified by in silico analysis were functional binding sites for some of the steroid receptors including AR, PR, and GR. Potential steroid target genes were identified in the vicinity of perfect HRE sequences. We expect our strategy will be useful for further studies of gene regulation and the elucidation of the steroid hormone receptor-mediated gene network that exerts distinct physiological and pathophysiological functions.

Acknowledgments

We thank Y. Suzuki and R. Nozawa for their technical assistance. This work was supported in part by Grants-in-Aid from the Ministry of Health, Labor and Welfare; from the Japan Society for the Promotion of Science. This work was supported in part by a grant of the Genome Network Project from the Ministry of Education, Culture, Sports, Science and Technology of Japan and for Development of New Technology from The Promotion and Mutual Aid Corporation for Private Schools of Japan.

References

[1] D.J. Mangelsdorf, C. Thummel, M. Beato, P. Herrlich, G. Schutz, K. Umesono, B. Blumberg, P. Kastner, M. Mark, P. Chambon, R.M. Evans, The nuclear receptor superfamily: the second decade, Cell 83 (1995) 835–839.

[2] M. Beato, P. Herrlich, G. Schutz, Steroid hormone receptors: many actors in search of a plot, Cell 83 (1995) 851–857.

[3] K. Horie-Inoue, H. Bono, Y. Okazaki, S. Inoue, Identification and functional analysis of consensus androgen response elements in human prostate cancer cells, Biochem. Biophys. Res. Commun. 325 (2004) 1312–1317.

[4] T. Hubbard, D. Andrews, M. Caccamo, G. Cameron, Y. Chen, M. Clamp, L. Clarke, G. Coates, T. Cox, F. Cunningham, et al., Ensembl 2005, Nucleic Acids Res. 33 (2005) D447–D453.

[5] H.U. Bono, SayaMatcher: Genome scale organization and systematic analysis of nuclear receptor response elements, Gene (2005). Available online August 24.

[6] P. Rice, I. Longden, A. Bleasby, EMBOSS: the European Molecular Biology Open Software Suite, Trends Genet. 16 (2000) 276–277.

[7] P.S. Nelson, N. Clegg, H. Arnold, C. Ferguson, M. Bonham, J. White, L. Hood, B. Lin, The program of androgen-responsive genes in neoplastic prostate epithelium, Proc. Natl. Acad. Sci. USA 99 (2002) 11890–11895.

[8] V. Matys, E. Fricke, R. Geffers, E. Gossling, M. Haubrock, R. Hehl, K. Hornischer, D. Karas, A.E. Kel, O.V. Kel-Margoulis, D.U. Kloos, S. Land, B. Lewicki-Potapov, H. Michael, R. Munch, I. Reuter, S. Rotert, H. Saxel, M. Scheer, S. Thiele, E. Wingender, TRANSFAC: transcriptional regulation, from patterns to profiles, Nucleic Acids Res. 31 (2003) 374–378.

[9] Y. Shang, M. Myers, M. Brown, Formation of the androgen receptor transcription complex, Mol. Cell 9 (2002) 601–610.

[10] V.E. Mick, O.A. Itani, R.W. Loftus, R.F. Husted, T.J. Schmidt, C.P. Thomas, The alpha-subunit of the epithelial sodium channel is an aldosterone-induced transcript in mammalian collecting ducts, and this transcriptional response is mediated via distinct cis-elements in the 5′-flanking region of the gene, Mol. Endocrinol. 15 (2001) 575–588.

[11] H. Vermeer, B.I. Hendriks-Stegeman, B. van der Burg, S.C. van Buul-Offers, M. Jansen, Glucocorticoid-induced increase in lymphocytic FKBP51 messenger ribonucleic acid expression: a potential marker for glucocorticoid sensitivity, potency, and bioavailability, J. Clin. Endocrinol. Metab. 88 (2003) 277–284.

[12] T.R. Hubler, W.B. Denny, D.L. Valentine, J. Cheung-Flynn, D.F. Smith, J.G. Scammell, The FK506-binding immunophilin FKBP51 is transcriptionally regulated by progestin and attenuates progestin responsiveness, Endocrinology 144 (2003) 2380–2387.

[13] A. Sandelin, W. Alkema, P. Engstrom, W.W. Wasserman, B. Lenhard, JASPAR: an open-access database for eukaryotic transcription factor binding profiles, Nucleic Acids Res. 32 (2004) D91–D94.

[14] X. Zhang, S. Firestein, The olfactory receptor gene superfamily of the mouse, Nat. Neurosci. 5 (2002) 124–133.

[15] M. Carpentier, C. Guillemette, J.L. Bailey, G. Boileau, L. Jeannotte, L. DesGroseillers, J. Charron, Reduced fertility in male mice deficient in the zinc metallopeptidase NL1, Mol. Cell. Biol. 24 (2004) 4428–4437.

[16] R. Urrutia, KRAB-containing zinc-finger repressor proteins, Genome Biol. 4 (2003) 231.1–231.8.

[17] E. Carballo, W.S. Lai, P.J. Blackshear, Feedback inhibition of macrophage tumor necrosis factor-alpha production by tristetraprolin, Science 281 (1998) 1001–1005.

[18] S. Cawley, S. Bekiranov, H.H. Ng, P. Kapranov, E.A. Sekinger, D. Kampa, A. Piccolboni, V. Sementchenko, J. Cheng, A.J. Williams, R. Wheeler, B. Wong, J. Drenkow, M. Yamanaka, S. Patel, S. Brubaker, H. Tammana, G. Helt, K. Struhl, T.R. Gingeras, Unbiased mapping of transcription factor binding sites along human chromosomes 21 and 22 points to widespread regulation of noncoding RNAs, Cell 116 (2004) 499–509.

THE JOURNAL OF BIOLOGICAL CHEMISTRY VOL. 281, NO. 19, pp. 13092–13102, May 12, 2006

17β-Estradiol Protects against Oxidative Stress-induced Cell Death through the Glutathione/Glutaredoxin-dependent Redox Regulation of Akt in Myocardiac H9c2 Cells*

Received for publication, March 1, 2006 Published, JBC Papers in Press, March 20, 2006, DOI 10.1074/jbc.M601984200

Yoshishige Urata[‡1,2], Yoshito Ihara[‡1], Hiroaki Murata[‡], Shinji Goto[‡], Takehiko Koji[§], Junji Yodoi[¶], Satoshi Inoue[‖], and Takahito Kondo[‡]

From the [‡]Department of Biochemistry and Molecular Biology in Disease, Atomic Bomb Disease Institute, Nagasaki University Graduate School of Biomedical Sciences, 1-12-4 Sakamoto, Nagasaki 852-8523, Japan, the [§]Department of Histology and Cell Biology, Nagasaki University Graduate School of Biomedical Sciences, 1-12-4 Sakamoto, Nagasaki 852-8523, Japan, the [¶]Department of Biological Responses, Institute for Viral Research, Graduate School of Medicine, Kyoto University, 53 Shogoin, Kawahara-cho, Sakyo-ku, Kyoto 606-8397, Japan, and the [‖]Department of Geriatric Medicine, Graduate School of Medicine, University of Tokyo, 7-3-1 Hongo, Bunkyo-ku, Tokyo 113-8655, Japan

The GSH/glutaredoxin (GRX) system is involved in the redox regulation of certain enzyme activities, and this system protects cells from H_2O_2-induced apoptosis by regulating the redox state of Akt (Murata, H., Ihara, Y., Nakamura, H., Yodoi, J., Sumikawa, K., and Kondo, T. (2003) *J. Biol. Chem.* 278, 50226–50233). Estrogens, such as 17β-estradiol (E_2), play an important role in development, growth, and differentiation and appear to have protective effects on oxidative stress mediated by estrogen receptor α (ERα). However, the role of the ERβ-mediated pathway in this cytoprotection and the involvement of E_2 in the redox regulation are not well understood. In the present study, we demonstrated that E_2 protected cardiac H9c2 cells, expressing ERβ from H_2O_2-induced apoptosis concomitant with an increase in the activity of Akt. E_2 induced the expression of glutaredoxin (GRX) as well as γ-glutamylcysteine synthetase, a rate-limiting enzyme for the synthesis of GSH. Inhibitors for both γ-glutamylcysteine synthetase and GRX and ICI182,780, a specific inhibitor of ERs, abolished the protective effect of E_2 on cell survival as well as the activity of Akt, suggesting that ERβ is involved in the cytoprotection and redox regulation by E_2. Transcription of the GRX gene was enhanced by E_2. The promoter activity of GRX was up-regulated by an ERβ-dependent element. These results suggest that the GRX/GSH system is involved in the cytoprotective and genomic effects of E_2 on the redox state of Akt, a pathway that is mediated, at least in part, by ERβ. This mechanism may also play an antiapoptotic role in cancer cells during carcinogenesis or chemotherapy.

Oxidative stress is a principle cause of the development of aging and diseases such as inflammation, infection, cancer, and cardiovascular disorders (1, 2). Exogenous or endogenous sources of oxidative stress and weakened antioxidative defenses can damage macromolecules such as DNA, lipids, and proteins.

Estrogens play an important role in development, growth, and the differentiation of both female and male secondary sex characteristics (3). Protective effects of estrogen, such as 17β-estradiol (E_2),[3] on oxidative stress have been indicated (4). E_2 regulates longevity signals to enhance resistance to oxidative stress in mice. Inhibitory effects of E_2 on atherosclerosis are mediated by COX-2-derived prostacyclin (5). E_2 induces production of antioxidative enzymes, such as superoxide dismutase (6), γ-glutamylcysteine synthetase (γ-GCS), and glutathione *S*-transferase (7). The effects of E_2 are mediated mostly through ERα, which functions as a ligand-induced transcription factor and belongs to the nuclear receptor superfamily (8). ERα binds to a variety of ligands and displays tissue-specific effects through estrogen-response element (ERE). When estrogen-responsive genes do not contain EREs, ERα can up-regulate gene expression through AP-1 and Sp1 sites (9). Another ER, ERβ, is expressed in cells targeted by E_2, including cardiomyocytes (10). However, the role of ERβ in protection against oxidative stress has not been well studied.

Protein thiols act as redox-sensitive switches and are believed to be a key element in maintaining the cellular redox balance. The redox state of protein thiols is regulated by oxidative stress and redox signaling and important to cellular functions. To maintain the cellular thiol-disulfide redox status, living cells possess two major systems, the thioredoxin (TRX)/TRX reductase system and the glutathione (γ-glutamylcysteinyl glycine, GSH)/glutaredoxin (GRX) system (11). GSH is synthesized in two sequential enzymatic reactions that are each catalyzed by a rate-limiting enzyme, γ-GCS, and GSH synthetase (12). GRX, also known as thioltransferase, was first discovered as a GSH-dependent hydrogen donor for ribonucleotide reductase in *Escherichia coli* mutants lacking TRX (13). Oxidized GRX is recycled to the reduced form by GSH with the formation of glutathione disulfide and regeneration of GSH by coupling with NADPH and glutathione disulfide reductase (14). GRX functions via a disulfide exchange reaction by utilizing the active site, Cys-Pro-Tyr-Cys, which specifically and efficiently catalyzes the reduction

* This work was supported in part by grants-in-aid for scientific research from the Ministry of Health, Labor, and Welfare of Japan (H15-Choju-015), by the Technology through the 21st Century Center of Excellence program, and by a research grant for health sciences from the Japanese Ministry of Health and Welfare. The costs of publication of this article were defrayed in part by the payment of page charges. This article must therefore be hereby marked "*advertisement*" in accordance with 18 U.S.C. Section 1734 solely to indicate this fact.

The nucleotide sequence(s) reported in this paper has been submitted to the GenBank™/EBI Data Bank with accession number(s) AF167981, BC063166, NM_001101.2, AY280663.1, U57439, NM_000125.2, and NM_001437.1.

[1] These authors contributed equally to this work.

[2] To whom correspondence should be addressed: Dept. of Biochemistry and Molecular Biology in Disease, Atomic Bomb Disease Institute, Nagasaki University Graduate School of Biomedical Sciences, 1-12-4 Sakamoto, Nagasaki 852-8523, Japan. Tel.: 81-95-849-7099; Fax: 81-95-849-7100; E-mail: urata@net.nagasaki-u.ac.jp.

[3] The abbreviations used are: E_2, 17β-estradiol; ER, estrogen receptor; ERE, estrogen-response element; GRX, glutaredoxin; γ-GCS, γ-glutamylcysteine synthetase; PP2A, protein phosphatase 2A; MTT, 3-(4,5-dimethyl-thiazole-2-yl)-2,5-diphenyltetrazolium bromide; HRP, horseradish peroxidase; PPT, propylpyrazoletriol; TBS, Tris-buffered saline; PDK1, 3-phosphoinositide-dependent protein kinase-1; TRX, thioredoxin; AMS, 4-acetamido-4′-maleimidylstilbene-2,2′-disulfonic acid; PBS, phosphate-buffered saline; RT, reverse transcription; BSO, buthionine sulfoximine; EpRE, electrophoretic response element.

of protein-SSG mixed disulfide (15). GRX also partially shares its function as a redox sensor with TRX (16, 17). Recently, we have found that GRX protects against oxidative stress-induced cell death from apoptosis by regulating the redox state of Akt (18).

Akt/protein kinase B is a pleckstrin homology domain-containing serine/threonine kinase and a critical component of an intracellular signaling pathway that exerts effects on survival and apoptosis (19). Akt has been found to be responsive to extracellular signaling factors, oxidative and osmotic stress, irradiation, and ischemic stress (20). Akt can phosphorylate Bad, caspase-9, and forkhead-related transcription factors, leading to an inhibition of apoptosis (21). The unphosphorylated form of Akt is virtually inactive, and phosphorylation at Thr^{308} and Ser^{473} stimulates its activity. Inactivation of Akt also occurs via dephosphorylation of the two phosphorylation sites by protein phosphatase 2A (PP2A) (22, 23). The activation of Akt contributes to the survival of H_2O_2-treated cells (24).

It has been reported that the function of ER-mediated transcriptional activity is regulated by redox (25). However, the precise mechanisms of redox regulation in the E_2-mediated signal pathways have not been clarified. Here we describe a mechanism for the antiapoptotic effect of E_2 through the regulation of the redox state of Akt under oxidative stress. Treatment of cardiac H9c2 cells with E_2 for 18 h protected against H_2O_2-induced apoptosis. E_2 induced the expression of GRX and γ-GCS, at least in part, through ERβ-mediated regulation. Elevated GSH and GRX levels potentiated the redox of Akt on the exposure of cells to H_2O_2.

MATERIALS AND METHODS

Reagents—Anti-PP2A scaffolding A subunit (PR65) antibody was obtained from Santa Cruz Biotechnology. Antibodies against human ERα (clone ER88) and ERβ (polyclonal) were from Kyowa Medex (Tokyo, Japan). Horseradish peroxidase (HRP)-conjugated goat anti-rabbit IgG F was purchased from MBL (Nagoya, Japan). HRP-goat anti-mouse IgG F was from Chemicon International (Temocula, CA). Normal goat IgG, normal rabbit IgG, and normal mouse IgG were from Sigma. Anti-Akt and anti-phospho-(Ser^{473})-Akt antibodies were from Cell Signaling Technology. Anti-PP2A catalytic C subunit antibody was from BD Transduction Laboratories. 3-(4,5-dimethyl-thiazole-2-yl)-2,5-diphenyltetrazolium bromide (MTT) was from Sigma. 4-Acetamido-4′-maleimidylstilbene-2,2′-disulfonic acid (AMS) was purchased from Molecular Probes, Inc. (Eugene, OR). H_2O_2 and $CdCl_2$ were from Wako Pure Chemicals (Osaka, Japan). ICI182,780 and propylpyrazoletriol (PPT) were from Tocris (Ballwin, MO).

Cell Culture—H9c2 cells, a clonal line derived from embryonic rat heart, and human breast cancer SK-BR-3 (SKB3) cells, and MDA-MB-231 (MDA) cells, were obtained from the American Type Culture Collection (CRL-1446). Human breast cancer MCF7 cells were from The Cell Resource Center for Biomedical Research Institute of Development, Aging, and Cancer, Tohoku University (Sendai, Japan). H9c2 cells were routinely maintained in Dulbecco's modified Eagle's medium, or MDA and SKB3 cells were maintained in RPMI1640 medium. The cells were supplied with 10% fetal calf serum in a humidified atmosphere of 95% air and 5% CO_2 at 37 °C (23).

Cell Viability—Cell viability was determined by a MTT assay as described (26). Briefly, cells (1500–5000) were placed in 100 μl of medium per well in 96-well plates. Four hours after treatment with various concentrations of H_2O_2, the cells were incubated for 4 h at 37 °C with 3-(4,5-dimethylthiazol-e-yl)-2,5-diphenyltetrazolium bromide (652 μg/ml) and lysed with 100 μl of 20% SDS, 50% *N*,*N*-dimethylformamide (pH 4.7) in each well. After an overnight incubation at 37 °C, the absorbance at 570 nm was measured. Wells without cells served as blanks.

Nuclear Condensation—For the histochemical analysis, cells were maintained in a four-well Lab Tec Chamber (Nalge Nunc International, Naperville, IL). After treatment with H_2O_2, cells were treated with 10 μM Hoechst 33342 for 30 min to estimate the extent of nuclear condensation. They were then washed again with PBS. Fluorescence intensity was examined using an Axioskop2 fluorescence microscope (Carl Zeiss, Jena, Germany), and the findings were analyzed using a charge-coupled device camera (Axio-Cam) and AxioVision software.

Morphological Staining—The immunohistochemical analysis to examine the expression of ERα and ERβ was performed as described previously (27). Briefly, cells were fixed with 4% paraformaldehyde in PBS and then preincubated with blocking solution for 1 h at room temperature. For ERβ 10% normal goat serum and 1% bovine serum albumin in PBS and for ERα 500 μg/ml of normal goat IgG and 1% bovine serum albumin in PBS were used, respectively. Next, the samples were incubated with the primary antibodies overnight and washed three times with 0.075% Brij 35 in PBS. Then samples were reacted with HRP-goat anti-mouse IgG or HRP-goat anti-rabbit IgG for 1 h at room temperature and washed three times with 0.075% Brij 35 in PBS. HRP sites were visualized with H_2O_2 and DAB solution or H_2O_2 and DAB in the presence of nickel and cobalt ions. As a negative control, normal rabbit IgG and normal mouse IgG were used instead of the primary antibodies. The results of immunohistochemistry for ERs were graded as positive or negative, compared with the staining with IgG or serum of a normal rabbit or mouse.

Immunoblot Analysis—Cultured cells were harvested and lysed for 20 min at 4 °C in lysis buffer as described previously (17). The supernatants obtained by centrifugation of the lysates at 8000 × *g* for 15 min were used in subsequent experiments. Protein concentrations were determined using a BCA assay kit (Pierce). Protein samples were electrophoresed on 10, 12.5, or 15% SDS-polyacrylamide gels under reducing conditions, except for thiol-modified protein samples. The proteins in the gels were transferred onto nitrocellulose membranes. The membranes were blocked in Tris-buffered saline (10 mM Tris-HCl (pH 7.5) and 0.15 M NaCl; TBS) containing 0.05% Tween 20 (v/v) (TBST) and 5% (w/v) nonfat dry milk and then reacted with primary antibodies in TBST containing 3% (w/v) bovine serum albumin overnight with constant agitation at 4 °C. After several washes with TBST, the membranes were incubated with horseradish peroxidase-conjugated anti-IgG antibodies. Proteins in the membranes were then visualized using the enhanced chemiluminescence detection kit (Amersham Biosciences) according to the manufacturer's instructions.

Akt Activity Assay—Akt activity was assayed using an Akt assay kit (Cell Signaling Technology) according to the manufacturer's directions with GSK3α/β fusion protein (GSK3α/β) as a substrate. Phosphorylation of GSK3α/β was assessed by immunoblot analysis using a specific antibody. Briefly, Akt was immunoprecipitated from cell lysates using the anti-Akt antibody, and then the immunoprecipitates were incubated at 30 °C for 30 min in an assay mixture containing GSK3α/β. Phosphorylated proteins were separated by 12.5% SDS-PAGE and then transferred to nitrocellulose membranes to detect phosphorylated GSK3α/β using an anti-phosphorylated GSK3α/β antibody.

Protein Phosphatase Assay—PP2A activity was assayed spectrophotometrically using a Ser/Thr phosphatase assay kit 1 (Upstate Biotechnology, Inc.) according to the manufacturer's instructions. The phosphopeptide RKpTIRR and *p*-nitrophenyl phosphate were used as phosphatase substrates.

Determination of Redox States—The redox states of proteins were assessed by modifying free thiol with AMS (28). Briefly, after incubation with or without H_2O_2, cell lysates or proteins were treated with trichloroacetic acid at a final concentration of 7.5% to denature and precipitate

the proteins as well as to avoid any subsequent redox reactions. The protein precipitates were collected by centrifugation at 12,000 × *g* for 10 min at 4 °C. The pellets were rinsed in acetone and centrifuged twice and then dissolved in a buffer containing 50 mM Tris-HCl (pH 7.4), 1% SDS, and 15 mM AMS. Proteins were then separated by 10% SDS-PAGE without using any reducing agents and blotted to nitrocellulose membranes. Proteins in the membranes were visualized by immunoblotting as described above.

Northern Blot Analysis—A 764-bp DNA fragment (bp 865–1628) of full-length γ-GCS heavy subunit cDNA was obtained by digestion with PstI (29). The probes were radiolabeled with ^{32}P using a random primer labeling kit (Takara Biomedicals, Shiga, Japan). The isolation of cytoplasmic RNA and Northern blotting were essentially performed as described by Sambrook *et al.* (30). Isolated RNAs (30 μg) were electrophoresed on a 1% agarose gel containing 0.6 M formaldehyde, transferred to a nylon membrane, and then hybridized with ^{32}P-labeled probes. Autoradiographed membranes were analyzed using a BAS5000 bioimage analyzer (Fuji Photo Film). A specific system for the amplification of mRNA was also used: an mRNA-selective PCR kit (Takara-Biomedicals; distributed by BioWhittaker, Europe). It had a total volume of 25 μl, comprising 12.5 μl of 2× buffer II, 5 mM $MgCl_2$, 0.5 μM PE1 and PE2, 1 mM each dNTP, 0.4 units of RNAsin (40 units/μl), 0.5 units of Rtase XL (5 units/μl), and 0.5 units of optimized Taq. As material, 1 μg of total RNA extracted from the cells was used. The 330-bp oligonucleotides for GRX (rat GRX sequence, accession number AF167981) were obtained using as a sense primer 5′-GCA TGG CTC AGG AGT TTG TGA ACT GCA AGA TTC AG-3′ and, as an antisense primer, 5′-CCT TTC ATA ACT GCA GAG CTC CAA TCT GCT TCA GC-3′. The 410-bp oligonucleotides for β-actin (rat β-actin sequence, accession number BC063166) were obtained using 5′-GAG CTA TGA GCT GCC TGA CG-3′ and 5′-AGC ATT TGC GGT GCA CGA TG-3′. The 410-bp oligonucleotides for β-actin (human β-actin sequence, accession number NM_001101.2) were obtained using 5′-GAG CTA CGA GCT GCC TGA CG-3′ and 5′-AGC ATT TGC GGT GCA CGA TG-3′. The 325-β oligonucleotides for ERα (rat ERα sequence, accession number AY280663.1) and 280-bp oligonucleotides for ERβ (rat ERβ sequence, accession number U57439) were obtained using 5′-GCT CTT GAC AAA CCC A-3′ and 5′-GCG GCG TTG AAC TCG TAG-3′ and 5′-GGC TGA GGA AAG CAC CTG TC-3′ and 5′-GCG GCG TTG AAC TCG TAG-3′, respectively. Similarly, the sense and antisense primers for the oligonucleotides for human ERα (accession number NM_000125.2) were 5′-GAC TAT GCT TCA GGC TAC C-5′ and 5′-GGT TCC TGT CCA AGA GCA AG-3′, whereas those for human ERβ (accession number NM_001437.1) were 5′-GTG GTC CAT CGC CAG TTA TC-3′ and 5′-GCA CTT CTC TGT CTC CGC AC-3′, respectively. The RT-amplification was carried out as follows: 30 min at 50 °C for the reverse transcription, denaturation for 5 min at 95 °C, and then a succession of 23 (35 for ERs) cycles as follows: 30 s at 95 °C, 40 s at 65 °C (55 °C for ERs), and 90 s at 72 °C. Amplification took place after 5 min at 72 °C.

Determination of Cellular Glutathione Levels—Total GSH and GSSG levels were measured using a total glutathione quantification kit (Dojindo Molecular Technologies, Inc.) according to the manufacturer's directions. Briefly, 5,5′-dithiobis-(2-nitrobenzoic acid) and GSH react to generate 2-nitro-5-thiobenzoic acid. The concentration of GSH in the sample solution was determined by measuring absorbance at 412 nm. For quantification of GSSG, cell lysates were treated with 2-vinylpyridine and triethanolamine to block the sulfhydryl residue of GSH. GSSG in the sample solution was reduced to GSH using a reducing mixture containing GSSG reductase and NADPH, and the levels of GSSG were determined photometrically as for GSH.

3-Phosphoinositide-dependent Protein Kinase-1 Activity—3-Phosphoinositide-dependent protein kinase-1 (PDK1) activity was estimated using an assay kit according to the manufacturer's instructions (Upstate Biotechnology). Briefly, recombinant human active PDK1 (Upstate Biotechnology) protein was incubated first with inhibitors for 30 min at 30 °C and then with inactive glucocorticoid-inducible kinase 1 (SGK1) for 30 min at 30 °C. Next, the PDK1-dependent SGK1 kinase activity was estimated by incubating the reaction mixture with glycogen synthase kinase 3 (GSK3) peptide as a substrate for 10 min at 30 °C in the presence of [γ-^{32}P]ATP.

Generation of Luciferase Reporter Constructs—A 2.0-kb fragment of the human GRX gene promoter (−2023 to −22) (31) was amplified by PCR using *Pfu* turbo DNA polymerase (Stratagene). The primers used were as follows: a forward primer (5′-GGA CTG AGT GAG AGG CAG ACA ATA GTC TCC-3′) and a reverse primer (5′-CGG GAA GAA TCC TCA GTT GCA GGT ATT GCT TGG-3′). The PCR product was subcloned into pUC18 to obtain pUC18-pro-GRX. PUC18-pro-GRX was digested with HindIII, and the resulting fragment containing the promoter region from −2023 to −22 was inserted into the HindIII site of the reporter vector pGL3-Basic (Stratogene) to give pGL3-pro-GRX. To generate a deleted version of the luciferase reporter construct (pGL3-pro-GRX-del), pGL3-pro-GRX was digested with KpnI and PvuII (Takara Biomedicals). Site-directed mutagenesis for luciferase vectors was performed with pGL3-pro-GRX (−2023 to −22) as a template by using a QuikChange site-directed mutagenesis kit (Stratagene). The oligonucleotides used were as follows: electrophoretic response element (EpRE)-like 1 forward (5′-GCT CCC CCT CCG GGA CTC AGA ATC TGG-3′) and EpRE-like 1 reverse (5′-CCA GAT TCT GAG TCC CGG AGG GGG AGC-3′). The nucleotide sequence was confirmed by sequencing with an ALFexpress II system (Amersham Biosciences).

Luciferase Activity Assay—Each vector was introduced into H9c2 cells by using Lipofectamine 2000 (Invitrogen) according to the manufacturer's instructions. After 12 h of transfection, cells were harvested for 24 h and then treated with E_2 (100 nM) or left untreated for 18 h. Then luciferase activity was assayed with cellular extracts by using a dual luciferase reporter assay system (Promega).

Electrophoretic Mobility Shift Assay—The electrophoretic mobility shift assay for the GC box and EpRE-like 1 element was performed as described (32). Briefly, oligonucleotides were annealed to double-stranded oligonucleotides and then labeled with [γ-^{32}P]ATP using T4 polynucleotide kinase. Oligonucleotides specific for the GC box and EpRE-like 1 element were prepared according to the nucleotide sequence of the human GRX promoter region. Oligonucleotides used were as follows: EpRE-like 1 element, 5′-CCC TCC GTG ACT CAG AAT CTG GCT TTC-3′; mutated EpRE-like 1 element, 5′-CCC TCC GGG ACT GTA AGC ACT TTA TGC TTC-3′. Binding reactions were performed in 15 μl of reaction mixture (25 mM Tris, pH 7.0, 6.25 mM $MgCl_2$, 0.5 mM EDTA, 0.5 mM dithiothreitol, 50 mM KCl, and 10% glycerol) containing 10 μg of nuclear extract and 25 ng of labeled oligonucleotide. For the supershift assay, specific antibodies were added to the reaction mixture during the binding reaction for 30 min.

Statistical Analysis—Data were presented as means ± S.D. Differences were examined by using Student's *t* test. A value of $p < 0.05$ was considered significant.

RESULTS

Expression of ERs—The expression of ERs in H9c2 cells was estimated immunohistochemically and genetically. Fig. 1 shows the results of the immunohistochemical analysis. Unlike MCF7 cells, which are known to express both ERα (Fig. 1*A*) and ERβ (Fig. 1*B*), H9c2 cells expressed ERβ (Fig. 1*F*) but not ERα (Fig. 1*E*). Fig. 1*I* shows the results of the RT-PCR

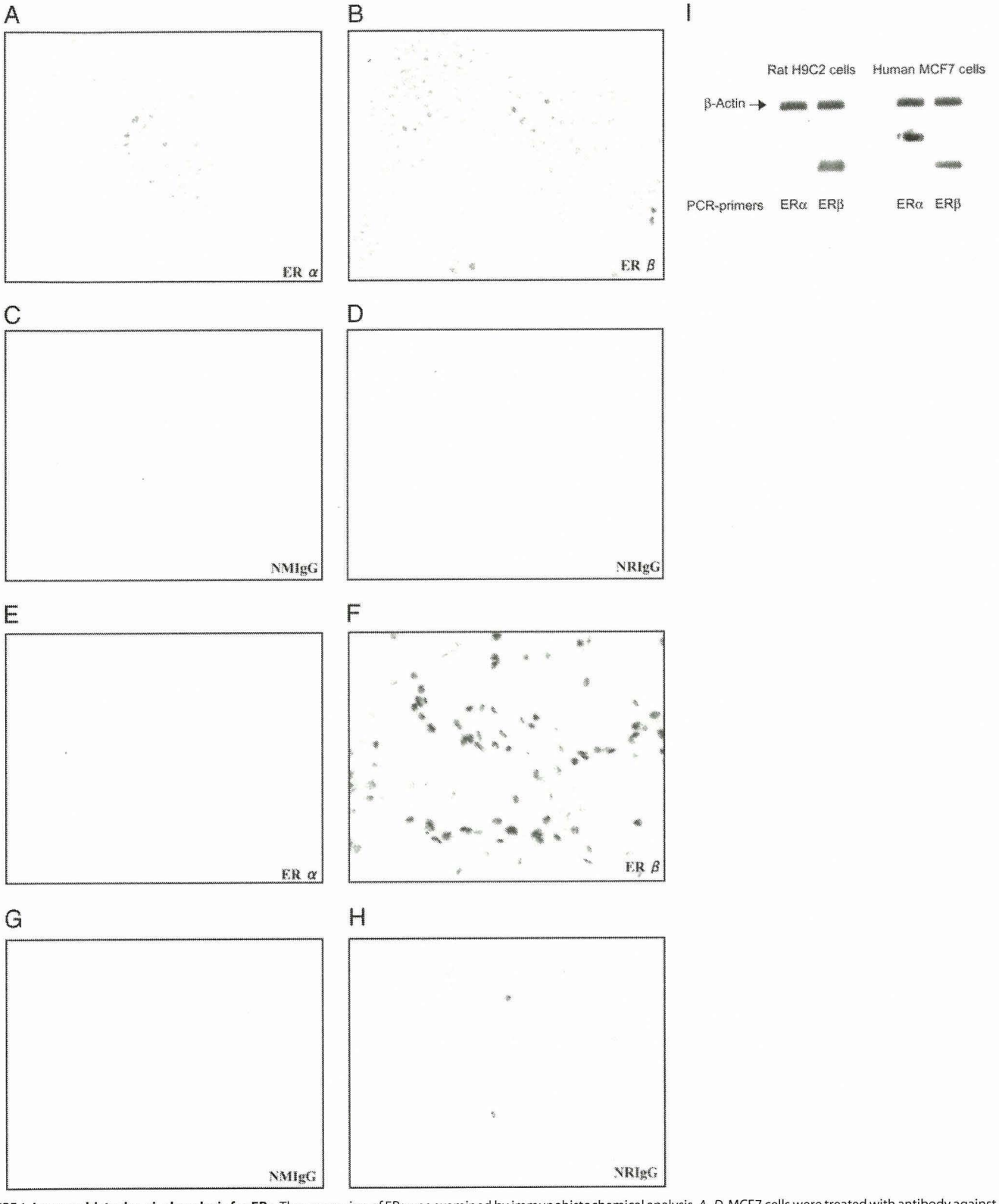

FIGURE 1. **Immunohistochemical analysis for ERs.** The expression of ERs was examined by immunohistochemical analysis. *A–D*, MCF7 cells were treated with antibody against ERα (*A*) and ERβ (*B*). *E–H*, H9c2 cells were treated with antibody against ERα (*E*) and ERβ (*F*). As a negative control, normal mouse IgG (*C* and *G*) or normal rabbit IgG (*D* and *H*) was used. The gene expression of ERs was examined by RT-PCR analysis (*I*) using sense-primers for rat ERα and -β mRNAs in H9c2 cells and those for human mRNA in MCF7 cells.

analysis. ERβ mRNA but not ERα mRNA was detected in H9c2 cells. On the other hand, both ER mRNAs were detected in MCF7 cells.

Cytoprotective Effect of E_2 on Oxidative Stress—We tested the cytoprotective effect of E_2 on oxidative stress-induced apoptosis in H9c2 cells. Hydrogen peroxide induces apoptosis or early mitochondrial dysfunction in cardiac H9c2 cells (32, 33). Since 10% fetal calf serum, required for maintaining cultured cells, reduces oxidative stress modification of cells, in order to observe the effect of E_2 on H_2O_2-induced oxidative stress, the concentration of fetal calf serum in the medium was changed from 10 to 0.5% in the experiments that followed. As shown in

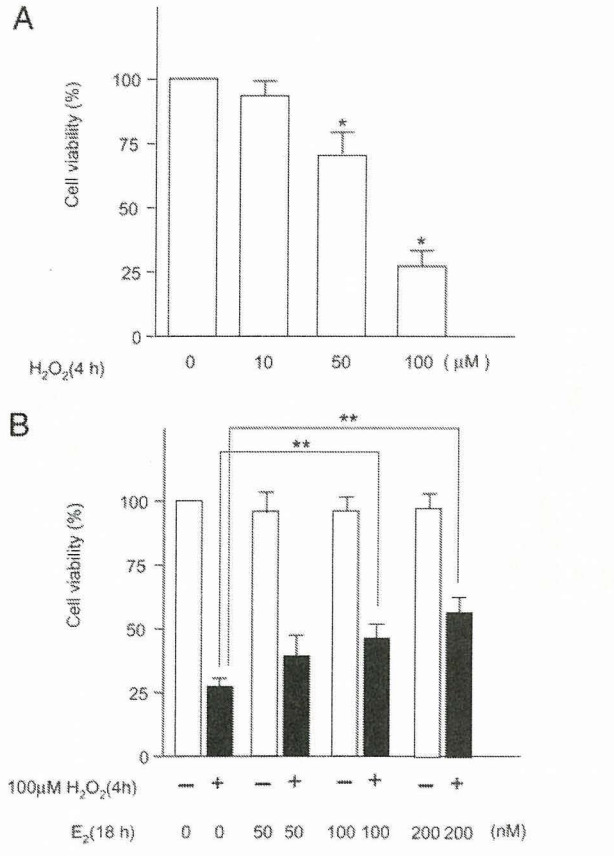

FIGURE 2. **Cytoprotective effect of E_2 on H_2O_2-induced apoptosis.** *A*, viability of H9c2 cells exposed to H_2O_2. Cells were treated with H_2O_2 (0–100 mM) for 4 h, and viability was estimated by the MTT assay. *B*, effect of E_2 on H_2O_2-induced apoptosis. Cells were treated with various concentrations (0–200 nM) of E_2 for 18 h and then with 100 mM H_2O_2 for 4 h. *C*, time course of the cytoprotective effect of E_2. Cells were treated with 100 nM E_2 for 0–36 h and then with 100 mM H_2O_2 for 4 h. The bars express viability (percentage) compared with the cells without H_2O_2. The data are mean ± S.D. of three independent analyses. *, $p < 0.05$ compared with untreated cells; **, $p < 0.05$ compared with cells with H_2O_2 without E_2.

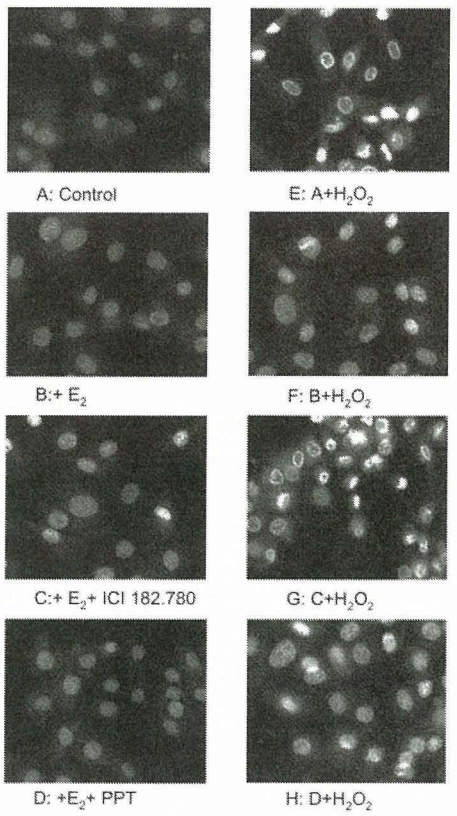

FIGURE 3. **H_2O_2-induced nuclear condensation.** Nuclear condensation was estimated from the PI staining. Cells were treated with 100 nM E_2 for 18 h with or without ICI182,780 (1 μM), a specific inhibitor of ERs, or 0.5 μM PPT (ERα agonist) and then with 100 μM H_2O_2 for 4 h. *A–D*, control cells; *B*, E_2; *C*, E_2 and ICI182,780; *D*, E_2 and PPT. *E–H*, cells treated with H_2O_2; *F*, E_2; *G*, E_2 and ICI182,780; *H*, E_2 and PPT.

Fig. 2*A*, the cell viability decreased by H_2O_2, as assessed photometrically with the MTT assay. The cell viability upon treatment with 100 μM H_2O_2 for 4 h was ~27% of the control. Prior treatment of the cells with 100 and 200 nM E_2 for 18 h prevented the H_2O_2 (100 μM)-induced cell damage by 1.4-fold and 1.8-fold of the control level, respectively (Fig. 2*B*). The increase in cell viability caused by E_2 observed in 18 h continued until 24 h and then declined until 36 h (Fig. 2*C*). Morphologically, H_2O_2-induced DNA condensation was observed (Fig. 3, *A versus E*). E_2 protected against DNA condensation (Fig. 3, *B versus F*). ICI182,780, an ER antagonist, abolished the protective effect of E_2 (Fig. 3, *C versus G*). PPT (0.5 mM), a specific inhibitor of ERα, had no apparent influence on the protective effect of E_2 (Fig. 3, *D versus H*). These results suggest that the protective effect against oxidative stress observed on treatment of the cells with E_2 for 18 h involves transcriptional regulation mediated by ERβ through a genomic pathway in this cell line. Unless otherwise indicated, subsequent experiments on the effect of E_2 were done by incubating the cells with 100 nM E_2 for 18 h.

E_2 Stimulated the Activity of Akt in Response to H_2O_2—The Akt cascade is known to mediate the survival function. The Akt signal is involved in both the genomic (34) and the nongenomic pathway of E_2 (35). We tested the involvement of Akt in the cytoprotective effect of E_2 in ERβ-positive H9c2 cells. Phosphorylation of Akt (Ser^{473}) was promoted by H_2O_2 in 10 min by 1.7-fold, and the control level was reached in 60 min (Fig. 4, *A* and *B*). Prior treatment with E_2 for 18 h resulted in a further increase in the H_2O_2-induced phosphorylation of Akt in 10 min by 4.1-fold, and the phosphorylation continued until 30 min (Fig. 4, *A* and *B*, *lanes 6 versus lanes 2* and *lanes 7 versus lanes 3*, respectively). ICI182,780 abolished the effect of E_2 (Fig. 4, *C* and *D*, *lanes 6 versus lanes 4*). The H_2O_2-induced enhancement of Akt activity estimated using GSK3α/β as a substrate was increased by E_2 (Fig. 4, *E* and *F*, *lanes 5 versus lanes 2* and *lanes 6 versus lanes 3*, respectively), concomitant with the increase in the phosphorylation of Akt. The activity of PDK1, upstream of Akt, was stimulated by H_2O_2; however, E_2 had no apparent effect on the activity of PDK1 (Fig. 4*G*). The phosphorylation of Akt is regulated by PP2A (18). The activity of PP2A assayed spectrophotometrically using RKpTIRR and *p*-nitrophenylphosphate as substrates was not affected by H_2O_2 and E_2 (Fig. 4*H*). The data suggest that the change in the activity of PP2A

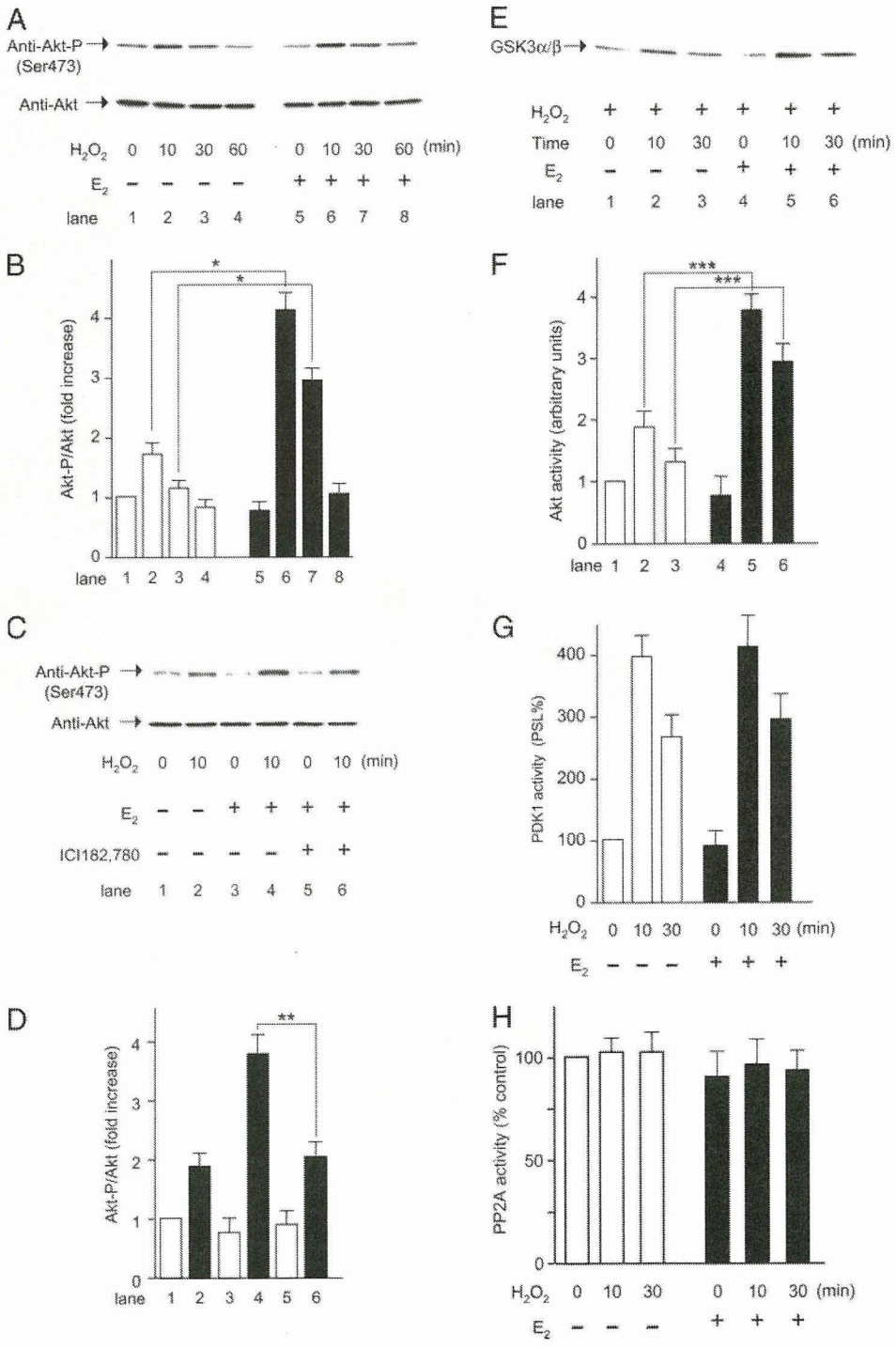

FIGURE 4. **Involvement of phosphorylation of Akt in the cytoprotective effect of E_2 against H_2O_2-induced apoptosis.** *A*, time course of Akt phosphorylation in H9c2 cells under oxidative stress. *C*, cells were treated with 100 nM E_2 in the presence or absence of 1 μM ICI182,780 for 18 h and then with 100 μM H_2O_2 for the period indicated. Phosphorylation of Akt was detected by immunoblot analysis using specific antibodies as described under "Materials and Methods." *B* and *D*, band intensity was estimated densitometrically, and the phosphorylation rates are expressed as the intensity of phosphorylated Akt relative to total Akt (*Akt-p/Akt*). *E*, activity of GSK3α/β. The kinase activity of Akt was measured based on the phosphorylation of GSK3α/β as described under "Materials and Methods." *F*, band intensity was estimated densitometrically, and the phosphorylation rates are expressed as arbitrary units. *G*, the activity of PDK1. The experimental conditions are the same as in *E*. *H*, the activity of PP2A. The activity of PP2A was measured as described under "Materials and Methods." The data are the mean ± S.D. of three independent analyses (*B*, *D*, and *F*). *, $p < 0.05$ compared with cells without E_2 at each time point; **, $p < 0.05$ compared with cells with H_2O_2 and E_2 without ICI182,780; ***, $p < 0.05$ compared with cells with H_2O_2 without E_2 at each time point.

is not involved in the up-regulation of the phosphorylation of Akt by E_2.

It has been reported that inactive Akt develops a redox-sensitive intramolecular disulfide bond close to its activation loop (18), and recently we found that the redox state of Akt is modulated by H_2O_2 (19). Fig. 5*A* shows the redox state of Akt assessed by modifying free thiol with AMS. In control cells, Akt existed mostly in an oxidized form (*lane 1*). Treatment of cells with H_2O_2 resulted in a further increase in an oxidized form of Akt (*lanes 2* and *3*). In the cells treated with E_2 for 18 h, Akt existed more in a reduced form (*lane 4*). The reduced form of Akt, once decreased by H_2O_2 for 30 min, was restored again in 60 min (*lanes 5* and *6*). The data suggested that E_2 maintains Akt in a reduced form under oxidative stress. The redox state of Akt is regulated by the GSH/GRX system, and this system protects cells against H_2O_2-induced apoptosis by preventing the association of Akt with PP2A (19). Then we estimated the effect of E_2 on the phosphorylation of Akt in the presence of buthionine sulfoximine (BSO), a specific inhibitor of γ-GCS, or cadmium, an inhibitor of GRX. γ-GCS is a rate-limiting enzyme of GSH synthesis. The effect of E_2 on the phosphorylation was abolished both by BSO (Fig. 5*B*) and by cadmium (Fig. 5*C*). These results suggest that E_2 increases the levels of GSH/GRX to protect cells against oxidative stress.

E_2 Induces the Expression of γ-GCS and GRX—We tested if E_2 increases the levels of GSH and GRX. E_2 increased the levels of GSH

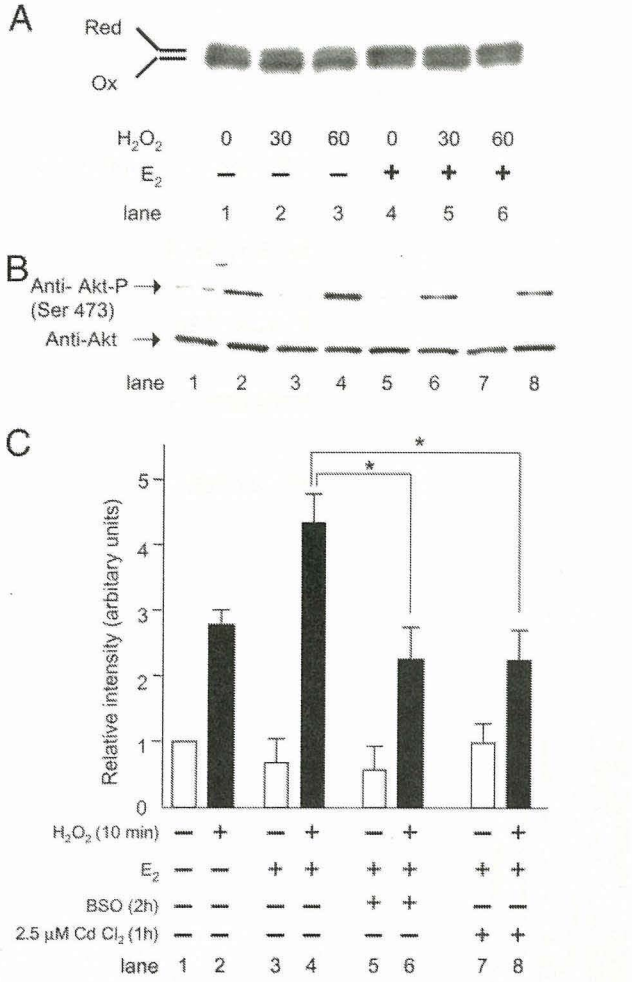

FIGURE 5. **E_2 retains the redox state of Akt.** *A*, the redox state of Akt was assessed based on mobility shifts of these proteins in an immunoblot analysis as described under "Materials and Methods." The positions of reduced (*Red*) and oxidized (*Ox*) proteins are indicated. The data are from a typical analysis. *B*, effect of modification of the redox on the phosphorylation of Akt was estimated, using 200 μM BSO, a specific inhibitor of γ-GCS (*lanes 5* and *6*), and 2.5 μM cadmium, an inhibitor of GRX (*lanes 7* and *8*). *C*, the activity of Akt phosphorylation is shown as relative intensity in the absence (*open bar*) and presence of H_2O_2 (*closed bar*). The data are the mean ± S.D. of three independent analyses. *, $p < 0.05$ compared with cells with H_2O_2 and E_2 without inhibitors.

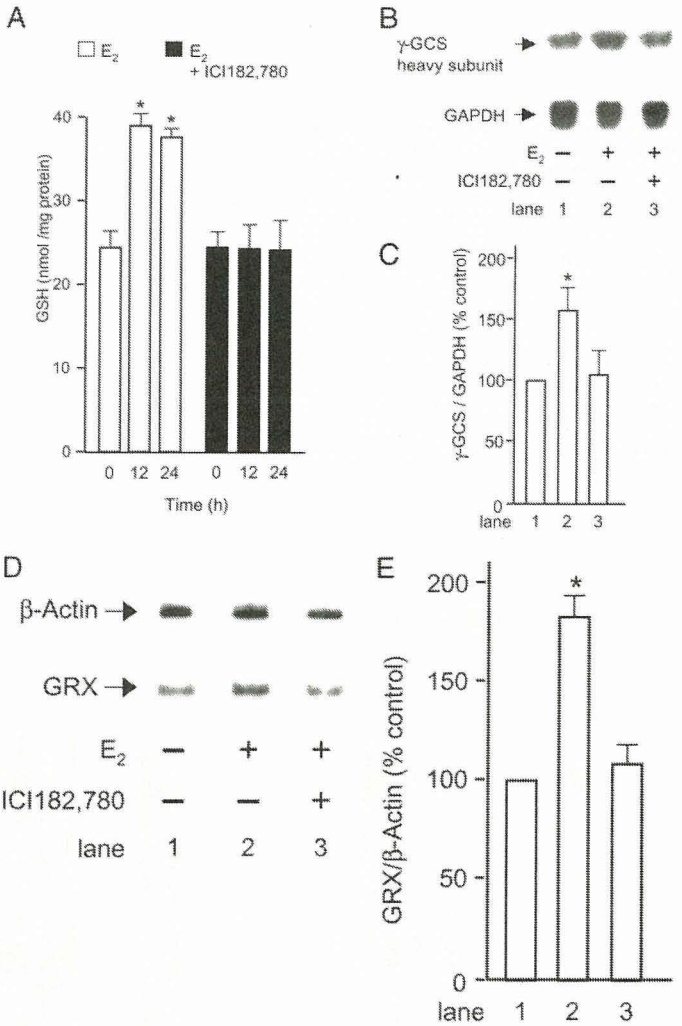

FIGURE 6. **GSH synthesis and GRX.** Effects of E_2 on levels of GSH, the γ-GCS heavy subunit, and GRX were estimated in the presence or absence of ICI182,780, as described under "Materials and Methods." *A*, cells were treated with 100 nM E_2 for 0–24 h, and the levels of GSH in the cell lysates were estimated. Cells were incubated with 100 nM E_2 for 6 h for the analysis of the expression of the γ-GCS heavy subunit by Northern blotting (*B*) and that of GRX by RT-PCR (*D*). The expression of γ-GCS was expressed as relative intensity (percentage of control) (*C*), and that of GRX was expressed as the intensity of GRX/β-actin (*E*). Each datum is a mean ± S.D. of three independent analyses. *, $p < 0.05$ compared with untreated cells.

(Fig. 6*A*). The level of GSH was 24.8 ± 4.0 nmol/10^6 cells in control cells and 38.5 ± 5.2 nmol/10^6 cells in cells treated with 100 nM E_2 for 18 h. The level of GSSG in the control cells was ~2 nmol/10^6 cells and was not changed by E_2 treatment (data not shown). The expression of γ-GCS was up-regulated by 100 nM E_2 by 1.6-fold in 18 h (Fig. 6, *B* and *C*). Similarly, 100 nM E_2 increased the expression of GRX by 1.8-fold in 18 h (Fig. 6, *D* and *E*). ICI182,780 abolished the E_2-dependent up-regulation of GSH synthesis as well as GRX synthesis (Fig. 6, *A–E*). It is suggested that the redox state of Akt is regulated by an E_2-dependent enhancement of the GRX/GSH system.

The Gene Promoter Activity of GRX Is Regulated by E_2 via an EpRE-like Element—As reported by Montano *et al.* (7), the expression of the γ-GCS heavy (catalytic) subunit is up-regulated by E_2 via an EpRE (5′-(G/A)TGACNNNGC(G/A)-3′), not by an ERE. To investigate the mechanism of the transcriptional regulation of GRX by E_2, we used a 2.0-kb genomic fragment containing the promoter region of GRX inserted into a luciferase vector, pGL3 Basic. The promoter region contains no apparent ERE or EpRE. There were two EpRE-like sites (EpRE-like 1 (−1380 to −1370; GTGACTCAGAA) and EpRE-like 2 (−347 to −337; GTGAGTAAGCA)) and Sp1 (−1217 to −1208, GCCCCGCCTC). The luciferase activity of the cells previously treated with E_2 for 18 h was almost lost when the EpRE-like 1 site was deleted or mutated (Fig. 7). Deletion of EpRE-like 2 or Sp1 had no apparent effect on the E_2-induced up-regulation of the luciferase activity.

E_2 Up-regulated the ERβ-EpRE-like 1 Complex Formation—To investigate the importance of the EpRE-like elements in the E_2-induced expression of GRX, an electrophoretic mobility shift assay was performed with nuclear extracts from the cells treated with E_2 for 18 h using ^{32}P-labeled oligonucleotides designed for EpRE-like 1. As shown in Fig. 8, a protein-DNA complex of EpRE-like 1 (*lane 2*) increased by E_2 (*lane 3*) and appeared in the presence of an excess of unlabeled probe (*lane 4*), or ^{32}P-labeled probe with the disabled mutant for EpRE-like 1 (*lane 5*). The addition of the anti-ERβ antibody caused the ERβ-DNA-binding complex to disappear (*lane 12*), indicating the involvement of ERβ as a transcription factor that bound to the EpRE-like 1 site. The EpRE-like 1 of GRX did not bind with Nrf2, Sp1, c-Jun, or c-Fos (*lanes 9–11*), different from the EpRE site of the γ-GCS heavy subunit (7). On the other hand, neither EpRE-like 2 site nor the Sp1 site was stimulated by E_2 (data not shown).